Bilirubin Conformational Analysis and Circular Dichroism

Richard V. Person, Blake R. Peterson, and David A. Lightner*

Contribution from the Departments of Chemistry and Biochemistry, University of Nevada, Reno, Nevada 89557-0020

Received July 19, 1993®

Abstract: Typical linear and porphyrin-like structure representations of bilirubin give an incorrect impression of its actual shape and expected solution properties. Conformational analysis of bilirubin, assisted by molecular dynamics computations, indicates that (i) nonbonded intramolecular steric interactions are minimized in a ridge-tile shape conformation lying at a global energy minimum on the conformational energy map and (ii) considerable additional stabilization is achieved through a network of intramolecular hydrogen bonds. The linear and porphyrin-like conformations are computed to lie some 37–48 kcal/mol above the isoenergetic global minimum energy conformations, which correspond to superimposable (identical) or to nonsuperimposable (enantiomeric) mirror image intramolecularly hydrogen-bonded ridge-tile conformers. Two different low-energy (19.5 and 21.4 kcal/mol) transition states can be identified on pathways for interconverting these conformational enantiomers. The conformation of bilirubin may be determined experimentally by UV–visible and, especially, circular dichroism (CD) spectroscopy. Such conformation dependent spectra arise from exciton coupling between the two dipyrrinone chromophores of bilirubin. Theoretical analysis using the exciton coupled oscillator model allowed a mapping of CD $\Delta\epsilon$ for each bilirubin conformation of the conformational energy surface. An intense bisignate CD spectrum is predicted for the global energy minimum conformation with Cotton effects $\Delta\epsilon \simeq \pm 200$ L mol^{-1} cm^{-1} for the long wavelength UV–visible absorption near 450 nm. Surprisingly, Cotton effect sign reversals without inversion of molecular absolute configuration are predicted when the ridge-tile conformations are flattened somewhat into higher energy structures.

Introduction

Bilirubin, the amphiphilic and cytotoxic yellow-orange pigment of jaundice is an unsymmetrically-substituted tetrapyrrole dicarboxylic acid found characteristically in mammals and produced in copious quantities by catabolism of heme, principally from the hemoglobin of red blood cells.[1,2] Its constitutional structure (Figure 1) was elucidated by Fischer, Pleininger, and Weissbarth over 50 years ago through a combination of degradation, partial, and total synthesis.[3] They showed the molecule to be an unsymmetrically-substituted tetrapyrrole dicarboxylic acid consisting of two dipyrrole halves conjoined by a saturated $-CH_2-$ group. The two halves are almost identical mirror images, though covalently linked, can react more or less independently. Aside from a few minor details, such as Fischer's preference for the lactim tautomer (hydroxypyrrole) and an unspecified stereochemistry at the C_4 and C_{15} carbon–carbon double bonds, the primary structure remains unchanged today. We now know that the lactam tautomer predominates in the constitutional structure[4] and, stemming principally from studies on jaundice phototherapy, we know that the natural pigment has the *Z* stereochemistry at the C_4 and C_{15} carbon–carbon double bonds.[5] In comparison with the stable (4*Z*,15*Z*) diastereomer, the other three possible diastereomers, (4*Z*,15*E*), (4*E*,15*Z*), and (4*E*,15*E*) are much less stable and revert easily to the (4*Z*,15*Z*) isomer. They have been seen only in studies of bilirubin photochemistry and in phototherapy.[5]

Fischer's structure is consistent with many properties of bilirubin—for example, a yellow color and solubility in dilute aqueous alkali. But it is inconsistent with many other properties

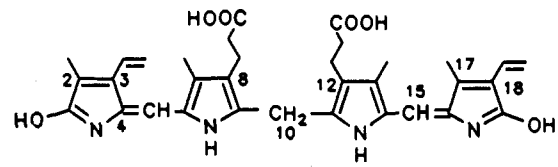

Figure 1. Fischer's structure of bilirubin (1941).

of the molecule, such as its high oil–water partition coefficient,[6] its resistance to hepatobiliary excretion[7] and—unusual for a carboxylic acid—its insolubility in aqueous sodium bicarbonate solution.[5] The reason for the apparent inconsistency is that Fischer's structure represents only the *constitutional structure* of bilirubin, not the three-dimensional structure or conformation. For bilirubin chemistry and metabolism, however, three-dimensional shape is crucially important. Yet, except in a few special circumstances,[8-10] until recently little was known with the required certainty of this most important aspect of structure.

Normal human metabolism generates some 300 mg/day/individual of bilirubin through the daily breakdown of about 10^{11} red blood cells.[1,2] Bilirubin is intrinsically unexcretable, and its secretion into bile is accomplished following its hepatic conjugation with glucuronic acid. Impaired secretion of bilirubin may indicate, *inter alia*, a pathologic liver condition, *e.g.*, cirrhosis or hepatitis, a blockage of the common bile duct (as in gallstones) or an insufficiency of bilirubin glucuronyl transferase (as in neonatal

* Abstract published in *Advance ACS Abstracts*, November 15, 1993.

(1) *Bile Pigments and Jaundice*; Ostrow, J. D., Ed.; Marcel-Dekker: New York, 1986; and references therein.

(2) For recent reviews, see: Pathobiology of Bilirubin and Jaundice. In *Seminars in Liver Disease*; Gollan, J. L., Guest Ed.; 1988; Vol. 8, Parts 2 and 3.

(3) Fischer, H.; Plieninger, H.; Weissbarth, O. *Hoppe-Seyler's Z. Physiol. Chem.* **1941**, *268*, 197–226.

(4) Falk, H.; Grubmayr, K.; Thirring, K., Gurker, N. *Monatsh. Chem.* **1978**, *109*, 1183–1189.

(5) Lightner, D. A.; McDonagh, A. F. *Acc. Chem. Res.* **1984**, *13*, 417–424 and references therein.

(6) McDonagh, A. F.; Lightner, D. A. *Pediatrics* **1985**, *75*, 443–455.

(7) McDonagh, A. F.; Lightner, D. A. The Importance of Structure in Bilirubin Metabolism and Excretion, In *Hepatic Metabolism and Disposition of Endo and Xenobiotics*; Bock, K. W., Gerock, W., Matern, S., Eds.; Falk Symposium No. 57, Kluwer, Dordrecht, The Netherlands, 1991; Chapter 5, pp 47–59.

(8) Bonnett, R.; Davies, J. E.; Hursthouse, N. B.; Sheldrick, G. M. *Proc. R. Soc. London, Ser. B* **1978**, *202*, 249–268.

(9) LeBas, G.; Allegret, A.; Mauguen, Y.; DeRango, C.; Bailly, M. *Acta Crystallogr., Sect. B* **1980**, *B36*, 3007–3011.

(10) Becker, W.; Sheldrick, W. S. *Acta Crystallogr., Sect B* **1978**, *B34*, 1298–1304.

(11) Brodersen, R. Aqueous Solubility, Albumin Binding and Tissue Distribution of Bilirubin. In *Bile Pigments and Jaundice*; Ostrow, J. D., Ed.; Academic Press: New York, 1986; p 158) has estimated K_{sp} for bilirubin in water at 37 °C to be $\sim 3 \times 10^{-15}$ M.

0002-7863/94/1516-0042$04.50/0

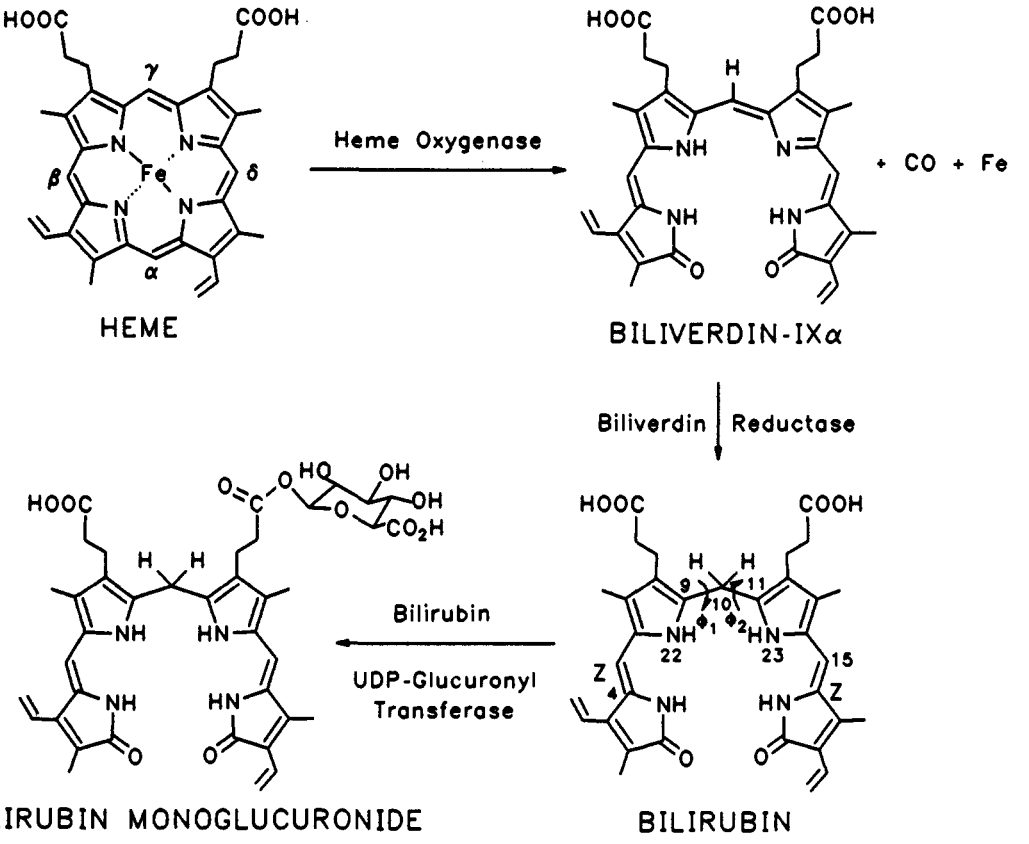

Figure 2. Metabolic steps in the production of bilirubin and conversion to a monoglucuronide. Both mono- and diglucuronides are formed and secreted across the liver into bile, but unconjugated bilirubin is not secreted into bile. Bilirubin is drawn in the porphyrin-like representation.

jaundice).[2] In the last, irreversible brain damage may result. What limits the facile excretability of bilirubin is its poor water solubility (estimated $K_{sp} \sim 3 \times 10^{-15}$ M for bilirubin in water at 37 °C),[11] high lipid/water partition coefficient[6] and proclivity to form association complexes with serum albumin and other protein[1,2,6,11,12]—three interrelated properties that dominate the transport and metabolism of the pigment *in vivo*.[1,2,13]

The interesting biological and unusual solubility properties of bilirubin do not correlate well, however, with either the porphyrin-like structure (Figure 2) or with the more conventional linear representation (Figure 3). If bilirubin adopted such conformations, which we now know are sterically disfavored, it would be predictably polar, not lipophilic and very likely excretable across the liver into bile without resort to glucuronidation.[7] The unusual properties of bilirubin are shared by its analogs having methyl and vinyl groups positioned symmetrically at C_2, C_3, C_{17}, and C_{18} and by analogs with vinyls reduced to ethyls, as in mesobilirubin-XIIIα (Figure 3). They can be ascribed, at least in part, to the location of propionic acid groups specifically at C_8 and C_{12}. Transposing the propionic acid groups with the adjacent methyl groups at C_7 and C_{13} yields a pigment, *e.g.*, mesobilirubin-IVα,[14] that is more polar and excretable without requiring glucuronidation or other structural modification.[7] Had Nature chosen to catabolize heme by oxidation at the β, γ, or δ positions instead of α (Figure 2), she would have produced bilirubins-IXβ, -γ, or -δ, which do not have propionic acid groups at C_8 and C_{12} and which are known to be more polar than the natural IXα isomer and readily excreted.[15]

The precise location of the propionic acid groups as a determinant of chemical, biological, and physical properties is, however, only one important structural requirement. Other stereochemical determinants include configuration and conformation of the tetrapyrrole skeleton—elements of three-dimensional structure which are shared by all of the pigments mentioned above. In the following, we describe and quantify the three-dimensional structure of bilirubin from molecular dynamics-assisted conformational analysis, relating our results to a unique structural type. We also assess the energetics associated with alteration of the conformation and shape of the molecule away from this type. Since circular dichroism (CD) and UV–visible spectroscopy have proven to be extremely sensitive probes of bilirubin chemistry and binding to proteins, we also computed these spectra, in the exciton chirality formulation,[16,17] for the entire range of conformations. We then show how the computed spectra may be compared with experimentally-determined spectra to distinguish pigment conformations in solution. As an experimental determinant of the importance of intramolecular hydrogen bonding to three-dimensional stereochemistry, synthetic bilirubin analogs are described in which intramolecular allosteric effects force their resolution into conformational enantiomers. These results are important because they provide a comprehensive picture of the probable shape and stereochemistry of bilirubin, they describe the energy requirements for assuming various three-dimensional shapes, and they predict a relationship between CD spectra and pigment conformation—as might be found when bound to proteins such as albumin.[18,19]

(12) McDonagh, A. F. Bile Pigments: Bilatrienes and 5,15-Biladienes, In *The Porphyrins*; Dolphin, D., Ed.; Academic Press: New York, 1979; Vol. 6, pp 293–491.
(13) *Bilirubin*; Heirwegh, K. P. M.; Brown, S. B., Eds.; CRC Press: Boca Raton, FL, 1982; Vols. 1 and 2, references therein.
(14) Trull, F. R.; Franklin, R. W.; Lightner, D. A. *J. Heterocycl. Chem.* **1987**, *24*, 1573–1579.
(15) Blanckaert, N.; Heirwegh, K. P. M.; Zaman, Z. *Biochem. J.* **1977**, *164*, 229–236.
(16) Lightner, D. A.; Gawroński, J.; Wijekoon, W. M. D. *J. Am. Chem. Soc.* **1987**, *109*, 6354–6362.
(17) Harada, N.; Nakanishi, K. *Circular Dichroic Spectroscopy-Exciton Coupling in Organic Chemistry*; University Science Books: Mill Valley, CA, 1983.
(18) Lightner, D. A.; Wijekoon, W. M. D.; Zhang, M-H. *J. Biol. Chem.* **1988**, *263*, 16 669–16 676 and references therein.
(19) Blauer, G. *Isr. J. Chem.* **1983**, *23*, 201–209, and references therein.

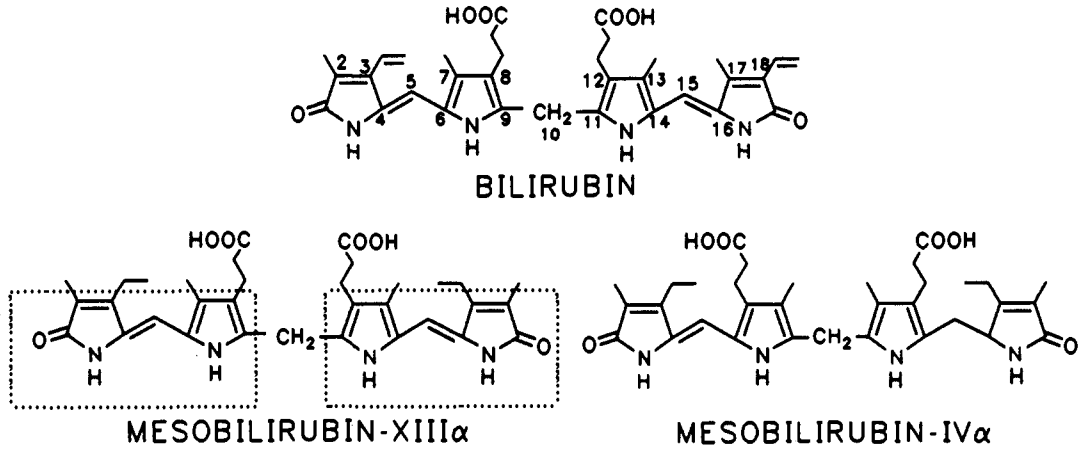

Figure 3. Linear representations for bilirubin and two symmetric synthetic analogs. Dipyrrinone units (chromophores) common to all three pigments are shown in dashed boxes on mesobilirubin-XIIIα.

Results and Discussion

Bilirubin Conformational Analysis. Like diphenylmethane[20] and dipyrrylmethanes[21-24] bilirubin and its analogs may be viewed as molecular propellers with two blades, each being a dipyrrinone chromophore (Figures 3 and 4C) connected to and capable of rotating independently about the central $-CH_2-$ group at C_{10} (Figure 4D). Such rotations sweep out large spatial volumes, creating a potentially infinite number of diverse conformations for these propellers, with a vast array of differing conformational energies and interconversion barriers. To complicate the picture, the longer dipyrrinone blades have at least one recognizable degree of conformational freedom not available in the simpler systems: the potential for curvature brought about by twisting the C_5–C_6 or C_{14}–C_{15} carbon–carbon single bonds (Figure 4C). (Rotations about the C_4 and C_{15} carbon–carbon double bonds are high-energy processes accessible by photoactivation.[25]) However, the conformational possibilities within the dipyrrinone blades are nonetheless severely limited by steric constraints, as indicated in earlier work involving both experiment[26] and CNDO/2-based force field calculations,[22,23] which find a strong preference for the *syn*-periplanar (*sp*) or *syn*-clinal (*sc*) conformations (Figure 4C). The *syn*-periplanar, with torsion angles 0–20°, predominates in crystalline bilirubin and mesobilirubin where intramolecular hydrogen bonding is adopted,[8-10] and in intermolecularly hydrogen-bonded dipyrrinone dimers.[22-24,26] The *syn*-clinal, with torsion angles 20–50° are favored by monomeric dipyrrinones with unsubstituted N–H groups.[22-24,26] In either case, the structural differences among such conformational isomers are small compared with those conformations generated through rotations of the dipyrrinone blades about the central $-CH_2-$ group at C_{10}.

In bilirubin, rotations of the dipyrrinone blades about the C_9–C_{10} and C_{10}–C_{11} carbon–carbon single bonds produce a wide variety of rather different and distinctive conformational structures. At the three extremes are the planar or nearly planar porphyrin-like, extended and linear conformations. They can be described or designated by their N_{22}–C_9–C_{10}–C_{11} and C_9–C_{10}–C_{11}–N_{23} torsion angles (ϕ_1 and ϕ_2, respectively). As arbitrary but convenient reference points, we designate the porphyrin-like conformation at $\phi_1 = \phi_2 \simeq 0°$, the linear conformation as $\phi_1 = \phi_2 \simeq 180°$, and the extended conformation as $\phi_1 = 0°$, $\phi_2 \approx 180°$ or $\phi_1 \simeq 180°$, $\phi_2 \simeq 0°$ (Figure 4D). Between these nearly planar conformations lie a very large number of nonplanar dissymmetric conformations, including some with near C_2 symmetry, each of which has a nonsuperimposable mirror image, as in conformations where $\phi_1 = \phi_2 \simeq 90°$ and where $\phi_1 = \phi_2 \simeq -90°$. (Near C_2 symmetry because the methyl and vinyl groups on the end rings are not symmetrically ordered. Mesobilirubin-XIIIα and mesobilirubin-IVα are symmetric and could therefore have C_2 symmetry nonplanar conformers.) Of course, the conformers are not all expected to be equal in energy. For example, as seen in CPK space-filled molecular models, the linear conformation is destabilized by a severe buttressing interaction between the propionic acid groups at C_8 and C_{12}; the porphyrin-like conformation is destabilized by nonbonded steric interactions between the lactam carbonyl groups; and the extended conformation is destabilized by severe nonbonded steric repulsions between the propionic acid groups and the pyrrole NH groups. However, between these limiting planar structural representations of bilirubin lie a collection of more stable conformers, as can be detected even in CPK space-filled models of bilirubin.

The relative energies and stabilities of the various conformations can be quantitated using molecular mechanics force field calculations. Thus, by using molecular dynamics in the SYBYL force field program, bilirubin conformations and their energies were computed and displayed as three-dimensional conformational energy maps, with potential energy (vertical axis) and ϕ_1 and ϕ_2 on the horizontal axes (Figure 5). A collection of isoenergetic global minima may be seen as deep "pot holes" in the conformational energy hypersurface, corresponding either to identical structures or to their enantiomeric mirror image, intramolecularly hydrogen bonded structures (labeled ***M*** and ***P*** in Figure 6). Here, the chirality of a helical propeller is denoted ***P*** (plus) for the right-handed configuration and ***M*** (minus) for the left. Satisfyingly, the SYBYL force field locates global energy minimum structures which are essentially identical to those seen in crystals of bilirubin and mesobilirubin by X-ray crystallography[8-10] and very similar to the conformations computed for bilirubin or its analogs using molecular orbital calculations.[22-24,27] In addition, and as might be expected, it will be shown later that the computed conformational energy map for the symmetric analog, mesobilirubin-XIIIα (Figure 3), is essentially identical to that of bilirubin, thus indicating that the presence and location of the end-ring vinyl substituents is relatively unimportant to the conformational energy map.

How similar are the molecular dynamics-generated global minimum bilirubin conformations to those found in crystals of

(20) Barnes, J. C.; Paton, J. D.; Damewood, J. R., Jr.; Mislow, K. *J. Org. Chem.* **1981**, *46*, 4975–4979.
(21) Favini, G.; Pltea, D.; Manitto, P. *Nouv. J. Chim.* **1979**, *3*, 299–301.
(22) Falk, H.; Müller, N. *Tetrahedron* **1983**, *39*, 1875–1885.
(23) Falk, H. *The Chemistry of Linear Oligopyrroles and Bile Pigments*; Springer Verlag: New York, 1989; references therein.
(24) Falk, H. Molecular Structure of Bile Pigments, In *Bilirubin*; Heirwegh, K. P. M., Brown, S. B., Eds.; CRC Press: Boca Raton, FL, 1982; Vols. 1 and 2, pp 7–29 and references therein.
(25) Lamola, A. A.; Braslavsky, S. E.; Schaffner, K.; Lightner, D. A. *Photochem. Photobiol.* **1983**, *37*, 263–270.
(26) Falk, H.; Grubmayr, K.; Höllbacher, G.; Hofer, O.; Leodolter, A.; Neufingerl, E.; Ribó, J. M. *Monatsh Chem.* **1977**, *108*, 1113–1130.
(27) Shelver, W. H.; Rosenberg, H.; Shelver, W. H. *Intl. J. Quantum Chem.* **1992**, *44*, 141–163.

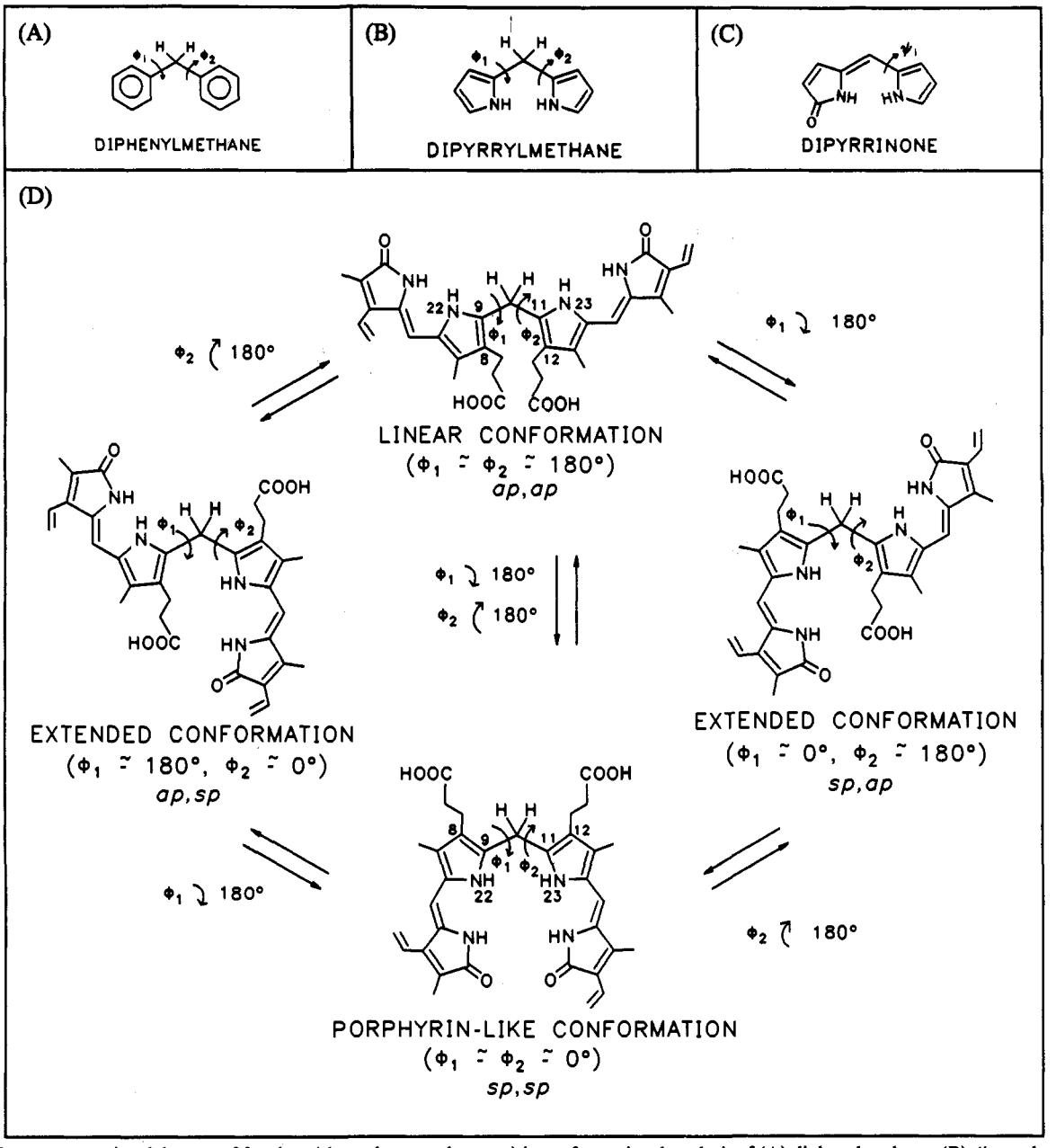

Figure 4. Important torsional degrees of freedom (shown by curved arrows) in conformational analysis of (A) diphenylmethane, (B) dipyrrylmethane, (C) the dipyrrinone chromophore shown in the *syn*-clinal or *syn*-periplanar conformation, and (D) bilirubin. (A), (B), and (D) may be viewed as molecular propellers. The planar (or nearly planar) bilirubin conformations are interrelated by rotations about torsion angles ϕ_1 [N_{22}–C_9–C_{10}–C_{11}] and ϕ_2 [C_9–C_{10}–C_{11}–N_{23}]. In our analyses, ϕ_1 and ϕ_2 are defined as 0° for the porphyrin-like conformation. Rotations about ϕ_1 and ϕ_2 by 180° convert the porphyrin-like conformation into the linear ($\phi_1 = \phi_2 \simeq 180°$) and to the extended ($\phi_1 \simeq 180°$, $\phi_2 \simeq 0°$ and $\phi_1 \simeq 0°$, $\phi_2 \simeq 180°$) conformations as well as to a multitude of helical conformations lying between and not shown here. The designations *sp* (*syn*-periplanar) and *ap* (*anti*-periplanar) refer to the rotational stereochemistry about C_{10}.

bilirubin by X-ray studies? In Table I it can be seen that the various torsion angles governing pigment shape are nearly identical. The picture in each case is one where two nearly planar dipyrrinone chromophores are rotated into a ridge-tile shape with an interplanar angle (θ) of ~100°. The double bonds at C_4 and C_{15} are not delocalized, and C_5–C_6 and C_{14}–C_{15} remain essentially single bonds about which rotation might occur so as to provide twist within the dipyrrinone chromophores. The propionic acid groups assume the staggered, fixed conformations associated with intramolecularly hydrogen bonding, and the nonbonded N–H···O=C and COOH···O=C distances fall within acceptable limits for hydrogen bonding. Molecular dynamics succeeds remarkably well in reproducing the structures found in crystals of bilirubin.

The unique structural type of Figure 6, intramolecularly hydrogen bonded enantiomeric three-dimensional conformers, appears to play a central role in explaining many of the properties of bilirubin. As a consequence of conrotating the two dipyrrinones in bilirubin or mesobilirubin to form a ridge-tile shape, the polar propionic acid carboxyl groups are brought into an ideal geometry for facile *intra*molecular hydrogen bonding. And with these polar groups tucked inward and tethered through such hydrogen bonding, bilirubin and mesobilirubin-XIIIα are rendered much more lipophilic than analogs where such internal sequestering of carboxyl groups is impossible—as in mesobilirubin-IVα (Figure 3), with its propionic acid groups relocated away from C_8 and C_{12}.

Interestingly, even in the absence of conformational stabilization through intramolecular hydrogen bonding, the minimum-energy conformation finds the dipyrrinones rotated into a ridge-tile shape in order to minimize nonbonded steric repulsions—into a position suitable for hydrogen bonding to the propionic acid carboxyl

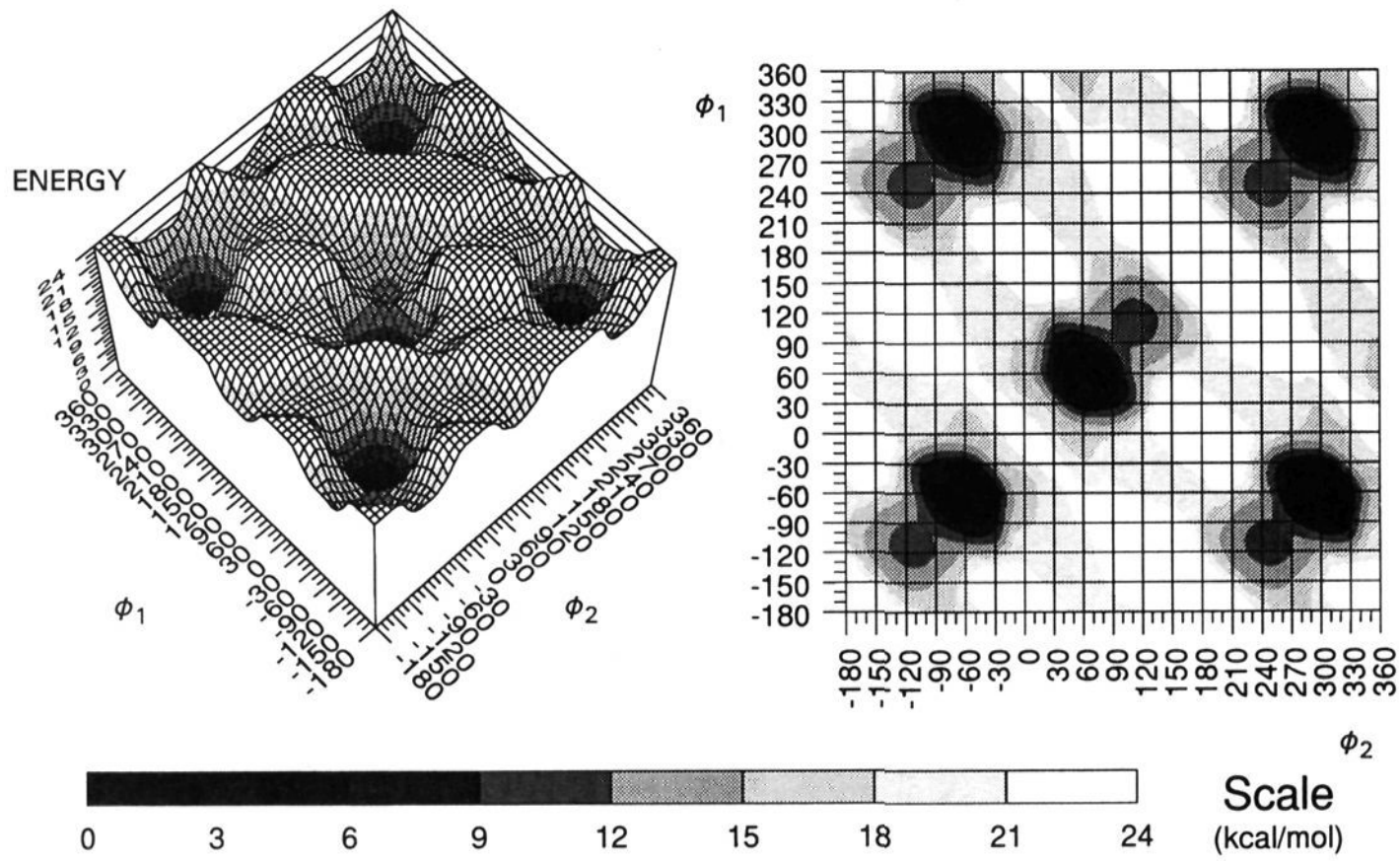

Figure 5. Conformational energy surface (left) and contour map (right) for bilirubin-IXα conformers generated by rotating the two dipyrrinone groups independently about the C_9–C_{10} and C_{10}–C_{11} carbon–carbon single bonds (ϕ_1 and ϕ_2, respectively) in steps of 10°. Isoenergetic global minima (set to 0.0 kcal/mol) are found near $\phi_1 = \phi_2 \simeq 60°$ (corresponding to the ***P***-chirality enantiomer) and near $\phi_1 = \phi_2 \simeq -60°$; $\phi_1 \simeq -60°$, $\phi_2 \simeq 300$; $\phi_1 \simeq 300°$, $\phi_2 \simeq -60°$ and $\phi_1 = \phi_2 \simeq 300°$ (all four corresponding to the ***M***-chirality enantiomer. Data are from molecular dynamics simulations using SYBYL (Tripos Assoc.) on an Evans & Sutherland ESV-10 workstation. The energy displays were created using Wingz (Informix).

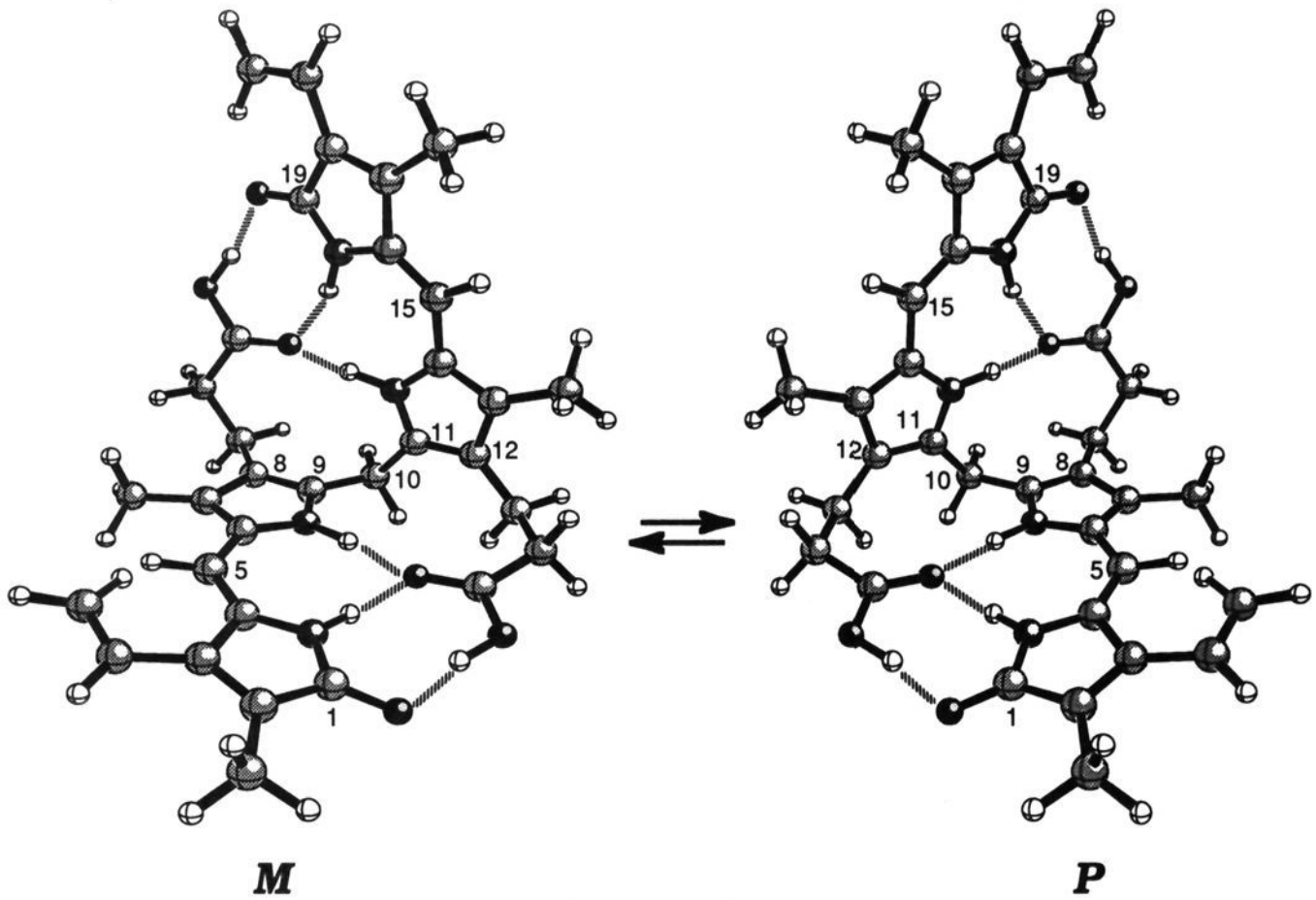

Figure 6. Ball and stick conformational representations for ridge-tile shape ***M***- and ***P***-chirality intramolecularly hydrogen-bonded interconverting enantiomers of bilirubin-IXα. These conformers correspond to the global energy minima identified in Figure 5 and are also depicted in Figure 11.

groups.[28] Although the rotation of the dipyrrinones into a folded, ridge-tile molecular geometry in bilirubins or mesobilirubin minimizes nonbonded steric repulsions, "turning on" intramolecular hydrogen bonding greatly lowers the global minimum energy, adding a powerful conformation-stabilizing force which is available in only a few tetrapyrrole conformations on the conformational energy surface of Figure 5. Consequently, the ability of bilirubin to adopt structures differing from the global energy minimum conformations (Figure 6) will depend on the energy available in the system under study. Although their independent existence might be improbable, higher energy conformations might be accessible to bilirubin by association complexation, *e.g.*, with proteins. Of course, the higher the energy of the bilirubin conformation (above the global minima), the less probable is its existence. Nevertheless, the fleeting existence or passing of unstable high-energy conformations seems assured because the ***M*** and ***P*** enantiomers (Figure 6) are able to interconvert at room temperature.

Interconversion of the ***M*** and ***P*** enantiomeric ridge-tile structures (Figure 6), stabilized through intramolecular hydrogen bonding, may be accomplished by rotating the dipyrrinones about

(28) Person, R. V.; Boiadjiev, S. E.; Peterson, B. R.; Puzicha, G.; Lightner, D. A. *4th International Conference on Circular Dichroism*; Sept 9–13, Bochum, FRG, 1991; pp 55–74.

Table I. Comparison of Representative Conformational Structure Parameters of Bilirubin as Found by Molecular Dynamics Calculations at a Global Minimum and as Found by X-ray Crystallography

torsion angle (deg) or distance (Å)	global min from molecular dynamics SYBYL ver 5.41	X-ray crystallography	
		Bonnett *et al.*[8]	Le Bas *et al.*[9]
N_{22}–C_9C_{10}–C_{11} (ϕ_1)	−59.1°	−59.8°	−63.3°
C_9–C_{10}–C_{11}–N_{23} (ϕ_2)	−58.9°	−63.7°	−60.6°
θ (dihedral angle)	85°	96°, 99°	97°
C_4–C_5–C_6–N_{22}	−9.7°	−17.5°	−7.8°
N_{23}–C_{14}–C_{15}–C_{16}	−10.0°	2.7°	−0.9°
N_{21}–C_4–C_5–C_6	−1.0°	10.7°	1.8°
C_{14}–C_{15}–C_{16}–N_{24}	−0.9°	−5.8°	1.3°
C_9–C_8–C_{8^1}–C_{8^2}	−122.7°	−118.4°	−113.5°
C_{11}–C_{12}–C_{12^1}–C_{12^2}	−122.7°		
C_8–C_{8^1}–C_{8^2}–C_{8^3}	67.8°	68.2°	67.9°
C_{12}–C_{12^1}–C_{12^2}–C_{12^3}	68.1°		
C_4–C_5	1.34 Å	1.30 Å	1.37 Å
C_{15}–C_{16}	1.34 Å	1.30 Å	1.37 Å
C_5–C_6	1.48 Å	1.48 Å	1.41 Å
C_{14}–C_{15}	1.48 Å	1.48 Å	1.42 Å
O_1–O_{19}	11.28 Å	11.13 Å	11.14 Å
O_1···HOOC	1.55 Å	1.58 Å	1.49 Å
O_{19}···HOOC	1.55 Å	1.58 Å	1.49 Å
C_{12^3}=O···HN_{22}	1.56 Å	1.81 Å	1.90 Å
C_{8^3}=O···HN_{23}	1.56 Å	1.81 Å	1.90 Å
C_{12^3}=O···HN_{21}	1.56 Å	1.70 Å	1.77 Å
C_{8^3}=O···HN_{24}	1.56 Å	1.70 Å	1.77 Å

the C_9–C_{10} and C_{10}–C_{11} bonds, torsion angles ϕ_1 and ϕ_2. In this equilibrium, two distinct lowest energy pathways, designated **A** and **B**, are evident in the three-dimensional conformational energy map of Figure 7 as illustrated for mesobilirubin-XIIIα. Path B has been the most widely accepted interconversion path for bilirubins. It takes the ***P***-chirality ridge tile conformation ($\phi_1 = \phi_2 \simeq 60°$) into its ***M***-chirality enantiomer at ($\phi_1 = \phi_2 \simeq -60°$) by climbing up a ridge and then crossing a saddle near $\phi_1 \simeq -60°$, $\phi_2 \simeq +60°$. This path consists of an initial rotation of one torsion angle from 60° through 0° and on to −60° with only minor changes in the second torsion angle. It is followed by conrotation of the second torsion angle from 60° through 0° to −60°. In the middle of this (near $\phi_1 = -60°$, $\phi_2 = 60°$ or $\phi_1 = 60°$, $\phi_2 = -60°$) path all six hydrogen bonds must be broken and reformed in the enantiomer. After they are broken, the energy can be stabilized through the middle of the path by the formation of one or two hydrogen bonds between the two propionic acid groups. The highest point on this path is 21.4 kcal/mol above the global minimum and corresponds to a conformation with the two propionic acid groups forming one hydrogen bond. (This barrier is actually higher than 21.4 kcal/mol because at some point in the path all hydrogen bonds are broken giving a true energy barrier of about 28.1 kcal/mol.) The conformational changes along path **B** are illustrated in the ball and stick drawings of Figure 8.

Interconversion of enantiomers along path **A** has not been recognized previously, but according to the present work this path is the lowest energy. Path **A** takes the ***P***-chirality enantiomer corresponding to the global minimum at $\phi_1 = \phi_2 \simeq 60°$ into the ***M***-chirality enantiomer corresponding to the isoenergetic global minimum at $\phi_1 \simeq 300°$, $\phi_1 \simeq -60°$. In slow motion, starting from $\phi_1 = \phi_2 \simeq 60°$, path **A** opens the dihedral angle, θ, symmetrically by ascending into a hanging valley and passing through a local minimum near $\phi_1 = \phi_2 \simeq 110°$. From this point ϕ_1 undergoes a steady positive rotation to 300°, while ϕ_2 continues on a steady negative rotation to −60°. While continuing to ascend a steep ridge, crossing a saddle near $\phi_1 = +180°$, $\phi_2 = +80°$ and slowly descending near points $\phi_1 = +230°$, $\phi_2 = +20°$ and $\phi_1 = +270°$, $\phi_2 = -20°$ before dropping steeply to the enantiomeric global minimum at ($\phi_1 = +300°$, $\phi_2 = -60°$). The changes in conformation along path **A** are illustrated by the ball and stick models of Figure 7. All three of the hydrogen bonds on one side of the molecule must be broken on this path, but none of the hydrogen bonds on the other side are broken. This means that all three hydrogen bonds on one half of the molecule may remain intact during the entire enantiomeric interconversion. As ϕ_1 continues in a positive direction, it looks like these hydrogen bonds help to reverse the direction of the ϕ_2 rotation and pull the rest of the molecule around to the opposite chirality. The energy barrier for this path is 19.5 kcal/mol, the lowest barrier for interconverting ***M*** and ***P*** chirality enantiomers.

Selected conformations at points along path **A** (Figure 9) and path **B** (Figure 8) illustrate the changes in shape that a bilirubin molecule would undergo during conformational inversion. Path **A**, in which only three hydrogen bonds are broken, is slightly lower energy (~2 kcal/mol) than path **B**, where all six hydrogen bonds are broken. The computed energy barriers for ***M*** ⇄ ***P*** conformational inversion (19.5 kcal/mol, path **A**; 21.4 kcal/mol path B) are gratifyingly close to that determined independently by two different ^{1}H NMR methods in $CDCl_3$ solvent: 18–20 kcal/mol[29-32] for rates of 7.2 ± 0.4 s^{-1} at ~53 °C[29] and 3–95 s^{-1} at 50–95 °C.[28-30]

The conformational inversion equilibrium between ***M*** and ***P*** enantiomers (Figures 6, 8, and 9) can be displaced toward one enantiomer or the other through the action of a chiral recognition agent, such as an optically active amine[16,33] or a protein,[18,19] which form noncovalent complexes with bilirubin or mesobilirubin. In bilirubin-IXα and mesobilirubin-XIIIα, which can form intramolecular hydrogen bonds—but not with mesobilirubin-IVα (Figure 3), which cannot—the net result of a displacement of the equilibrium is strong optical activity from the complexed pigment. Optical activity can be detected and measured by CD spectroscopy, as shown, for example in Figure 10. The CD intensity ($\Delta\epsilon$) is observed to vary considerably with the nature and binding affinity of the complexation agent, apparently reflecting the enantioselectivity of complexation and thus the extent to which the conformational enantiomer equilibrium of Figures 6 and 7 or 8 is displaced. The largest observed CD Cotton effect magnitudes are those in the presence of certain serum albumins, *e.g.*, $\Delta\epsilon \pm$ 250 M/cm for porcine serum albumin in aqueous buffer[34] and select, optically active amines, *e.g.*, $\Delta\epsilon \pm$ 210 M/cm for (−)-ψ-ephedrine methyl ether in benzene.[33] However, whether many of these particularly large observed $\Delta\epsilon$ values can be attributed to complete displacement of the conformational equilibrium toward one enantiomer has remained unconfirmed until recently, because no one has ever resolved bilirubin or mesobilirubin into its enantiomers and measured their CD spectra. This simple picture of the relationship between bilirubin optical activity measured by CD and displacement of the conformational equilibrium toward the ***M*** or ***P*** enantiomers may be inadequate, however, to explain recent investigations on the influence of volatile anesthetics on the CD of bilirubin–albumin complexes.[35,36] Subtle stereochemical changes at the binding site are apparently responsible for the complete inversion of the pigment CD Cotton effect signs following addition of general anesthetics such as halothane or chloroform. Since CD spectroscopy can serve potentially to elucidate not only the handedness of the bound pigment but also the local topography at its binding site on the protein, a more complete understanding of the relationship between pigment conformation and CD is required.

(29) Manitto, P.; Monti, D. *J. Chem. Soc., Chem. Commun.* **1976**, 122–123.
(30) Kaplan, D.; Navon, G. *Isr. J. Chem.* **1983**, *23*, 177–186.
(31) Kaplan, D.; Navon, G. *Biochem. J.* **1982**, *201*, 605–613.
(32) Navon, G.; Frank, S.; Kaplan, D. *J. Chem. Soc., Perkin Trans 2* **1984**, 1145–1149.
(33) Pu, Y.-M.; Lightner, D. A. *Croat. Chem. Acta* **1989**, *62*, 301–324.
(34) Harmatz, D.; Blauer, G. *Arch. Biochem. Biophys.* **1975**, *170*, 375–386.
(35) Pu, Y. M.; McDonagh, A. F.; Lightner, D. A. *Experientia* **1992**, *48*, 246–248.
(36) Pu, Y.-M.; McDonagh, A. F.; Lightner, D. A. *J. Am. Chem. Soc.* **1993**, *115*, 377–380.

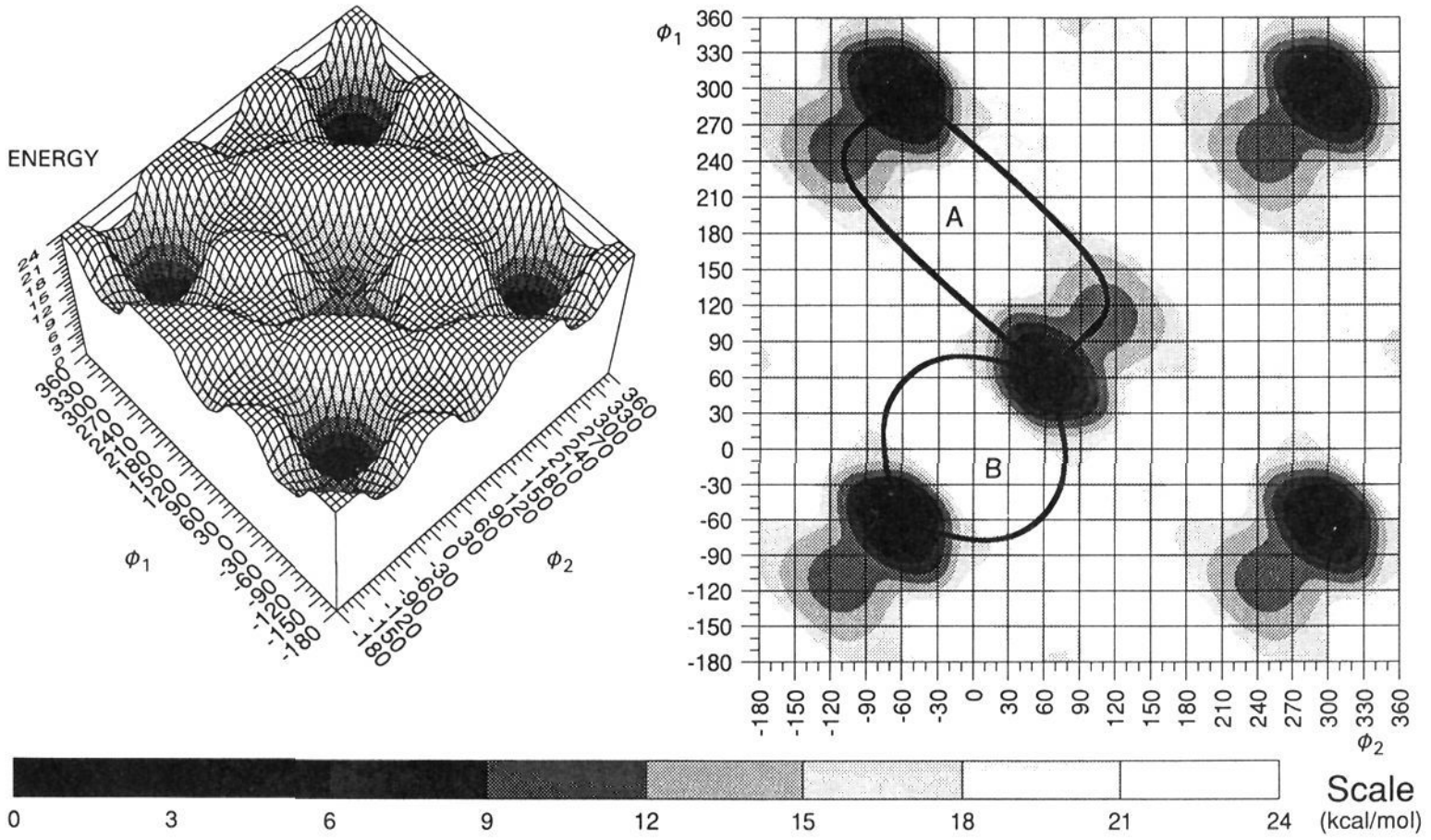

Figure 7. Conformational energy surface (left) and contour map (right) for mesobilirubin-XIIIα conformers generated by rotating the two dipyrrinone groups independently about the C_9–C_{10} and C_{10}–C_{11} carbon–carbon single bonds (ϕ_1 and ϕ_2, respectively) in steps of 10°. Isoenergetic global minima (set to 0.0 kcal/mol) are found near $\phi_1 = \phi_2 \simeq 60°$ (corresponding to the ***P***-chirality enantiomer) and near $\phi_1 = \phi_2 \simeq -60°$; $\phi_1 \simeq -60°$, $\phi_2 \simeq 300$; $\phi_1 \simeq 300°$, $\phi_2 \simeq -60°$ and $\phi_1 = \phi_2 \simeq 300°$ (all four corresponding to the ***M***-chirality enantiomer). Data are from molecular dynamics simulations using SYBYL (Tripos Assoc.) on an Evans & Sutherland ESV-10 workstation. Two lowest energy routes (A and B) connecting the ***M*** and ***P*** conformational enantiomers are identified on the topographic map (right), with barriers of 19.5 and 21.4 kcal/mol, respectively. Data, which are nearly identical to those of bilirubin-IXα (Figure 5), are from molecular dynamics. The energy displays were created using Wingz (Informix).

The Origin of Bilirubin Circular Dichroism: Bilirubin as a Molecular Exciton. The unusual bisignate CD spectra of Figure 10 derive from the fact that bilirubin and mesobilirubin are bichromophoric molecules, wherein two dipyrrinone chromophores are covalently linked by but not conjugated through the $-CH_2-$ group at C_{10}. Such CD spectra are characteristic of those produced by excited state induced electric dipole–dipole interaction (called exciton coupling) between two proximal (dipyrrinone) chromophores, each with strongly allowed UV–visible absorption in the region 400–450 nm and little orbital overlap between them.[16,17] Maximum exciton interaction between the intense long wavelength electronic transitions ($\epsilon_{420}^{max} \simeq 35\,000$) of each component dipyrrinone occurs when the chromophores are held ~90° apart, where interchromophoric orbital interaction (homoconjugation) is also minimized. This leads to strongly *allowed (intense) CD transitions. Such a favorable orientation* of dipyrrinone chromophores and hence their electric transition dipoles is found in the ridge-tile shape, intramolecularly hydrogen-bonded conformations (Figure 6) shown in Figure 11. When the ridge tile conformation closes up in the direction of the much higher energy (Figure 5) porphyrin-like conformation or unfolds in the direction of much higher energy extended or linear conformations, the transition dipoles tend to reorient toward parallel or in-line, respectively, and major changes in the UV–visible and CD spectra are predicted to accompany such conformational distortions.[28,37]

According to exciton coupling theory,[17,38] excited-state dipole–dipole interaction should lead to a splitting of the ~400–450 nm UV–visible band and accompanying oppositely signed CD Cotton effects for the two resultant exciton transitions. The splitting magnitude, the allowedness of each transition and the signed CD Cotton effect depend crucially on the relative orientation of the transition dipoles from each dipyrrinone—hence on the relative disposition of the dipyrrinones and thus the conformation of the bilirubin pigment. The porphyrin-like (Figure 4D), the ridge-tile (Figure 11), and the extended (Figure 4D) conformations closely resemble the classical cases for parallel, oblique, and in-line orientations of the induced electric dipole transition moments studied in detail by Kasha *et al.*[38] and illustrated in Figure 12. In the oblique orientation found in the ridge-tile conformation of Figures 6 and 11, both exciton transitions are predicted to be allowed—and both are in fact seen in the CD spectra as a bisignate Cotton effect (Figure 10). Their UV–visible spectrum appears as a broadened, sometimes split band at long wavelength.[16,18,33] With distortion of the ridge-tile conformation by closing down toward the porphyrin-like (Figure 4), which corresponds approximately to the parallel case of Figure 12, the UV–visible band is predicted to sharpen and blue-shift because the transition probability to the higher energy (shorter wavelength) exciton state increases, with a corresponding decrease in transition probability for the longer wavelength lower energy exciton state. In contrast, as the ridge-tile conformation is splayed open toward the linear or, especially, the in-line extended, the UV–visible band is expected to sharpen and red-shift as the transition probability to the lower energy, longer wavelength exciton state increases, while the transition probability to the higher energy exciton state decreases. Significantly, as the relative orientation of the dipyrrinone chromophores closes toward the porphyrin-like or stretches to the extended in-line or linear conformations (Figure 4), the allowedness of ***both*** CD exciton transitions *decreases* and orbital interaction between the chromophores can be expected to increase somewhat. Thus, the CD Cotton effects are predicted to be most intense in folded conformations and are expected to shrink and approach zero as the porphyrin-like and linear and extended conformations are accessed.

Computed Conformational Dependence of Circular Dichroism. Using the coupled oscillator formalism,[16,17] the CD and UV–visible spectra of mesobilirubin-XIIIα were computed for all of the conformations represented in the conformational energy map

(37) See Blauer, G.; Wagnière, G. *J. Am. Chem. Soc.* **1976**, *97*, 1949–1954.

(38) Kasha, M.; El-Bayoumi, M. A.; Rhodes, W. *J. Chim. Phys.-Chim. Biol.* **1961**, *58*, 916–925.

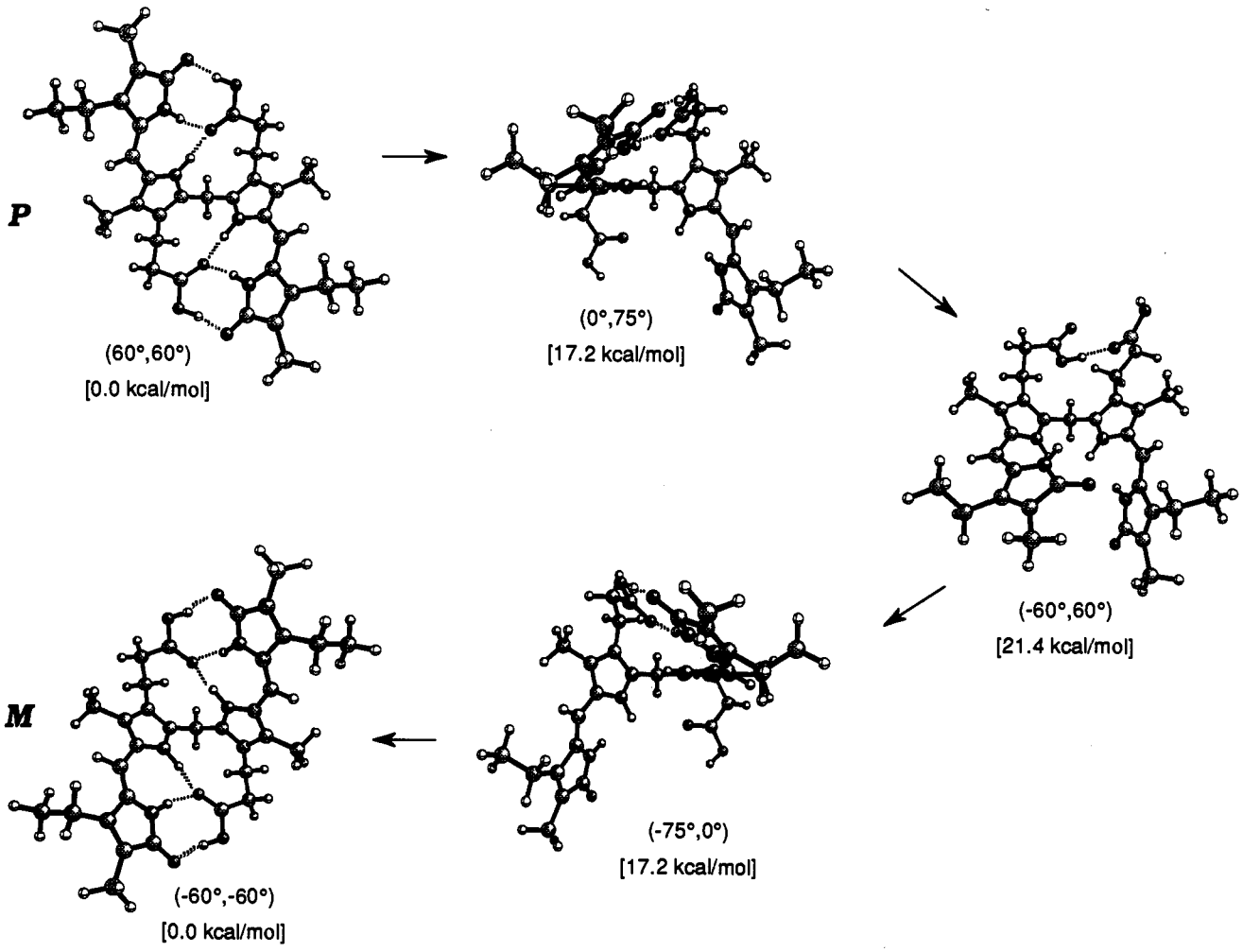

Figure 8. Ball and stick representations (defined by torsion angles (ϕ_1, ϕ_2) and energies [kcal/mol]) for mesobilirubin-XIIIα conformations lying along path B (Figure 7) for the interconversion of the *P* and *M* chirality global energy minimum enantiomeric conformers. The conformation ($\phi_1 \simeq -60°$, $\phi_2 \simeq 60°$) at the transition state for the interconversion lies some 21.4 kcal/mol above the global minima.

of Figure 7. The unscaled computed CD data are displayed as a three-dimensional graph in Figure 13, where $\Delta\epsilon$ for the lower energy long wavelength excitaton state is plotted on the vertical axis and conformational torsion angles ϕ_1 and ϕ_2 are plotted on the horizontal axes. (An essentially identical map would be obtained for bilirubin-IXα.) In Figure 13, a diagonal line connecting points ($\phi_1 = 360°$, $\phi_2 = 0°$) and ($\phi_1 = 0°$, $\phi_2 = 360°$) separates mirror image enantiomeric conformations. That is, conformations corresponding to points falling below the indicated diagonal line have nonsuperimposable mirror image conformations lying at points reflected across the diagonal. Reflection across the indicated diagonal thus inverts the sign (but not the magnitude) of the corresponding CD Cotton effect ($\Delta\epsilon$). In the case of bilirubin, for example, the conformation corresponding to the point $\phi_1 = +30°$, $\phi_2 = +270°$ has an enantiomer at $\phi_1 = +330°$, $\phi_2 = +90°$—with equal but oppositely signed bisignate CD Cotton effects. The conformation corresponding to the point $\phi_1 = +90°$, $\phi_2 = +330°$ is, strictly speaking, not an enantiomer of that at $\phi_1 = +30°$, $\phi_2 = +270°$, but for CD purposes it behaves like one. Due to its greater symmetry, the $\phi_1 = +30°$, $\phi_2 = +270°$ conformation of mesobilirubin-XIIIα would have an enantiomer at $\phi_1 = +330°$, $\phi_2 = +90°$ and at $\phi_1 = +90°$, $\phi_2 = 330°$. In a second example, the point $\phi_1 = \phi_2 \simeq +60°$ corresponds to the *P* enantiomer of Figures 6 and 11 and also to a global minimum structure. A *positive* $\Delta\epsilon$ is computed for the lower energy longer wavelength half of the bisignate CD curve. Reflection of this point across the indicated diagonal gives the new point ($\phi_1 = \phi_2 \simeq +300°$), which corresponds to the mirror image *M* enantiomer having a computed *negative* $\Delta\epsilon$ for the longer wavelength half of the bisignate CD curve.

More interestingly, the graph of computed CD Cotton effect $\Delta\epsilon$ maxima also shows that *the sign of* $\Delta\epsilon$ *can become inverted without an inversion of molecular chirality*. That is, when ϕ_1 and ϕ_2 increase, *e.g.*, from $\phi_1 = \phi_2 \simeq +60°$, the magnitude of $\Delta\epsilon$ is computed to decrease to zero for conformations corresponding to points ϕ_1, ϕ_2 lying near a contour line running roughly from $\phi_1 = 180°$, $\phi_2 \simeq 0°$ to $\phi_1 \simeq 0°$, $\phi_2 = 180°$ and passing through $\phi_1 = \phi_2 \simeq 120°$. In the region above this contour, the sign of $\Delta\epsilon$ reverses, and its magnitude gradually increases then rapidly decreases back to zero for conformations at points lying along a diagonal line running between $\phi_1 = 360°$, $\phi_2 = 0°$ and $\phi_1 = 0°$, $\phi_2 = 360°$. This line separates enantiomeric conformations. The changes in $\Delta\epsilon$ along the diagonal path connecting points $\phi_1 = \phi_2 = 0°$ and $\phi_1 = \phi_2 = 360°$ are illustrated in Figure 14, which displays not only $\Delta\epsilon$ (black line) but also the conformational potential energy (grey line) values (taken from Figures 13 and 5, respectively). Although $\phi_1 = \phi_2$ points where ϕ_1 and ϕ_2 lie between 0° and 180° correspond to various conformations with the same molecular chirality, conformational changes with no change in absolute configuration are predicted to afford either the expected (+)-exciton chirality or the unexpected (–)-exciton chirality CD. Similarly, although $\phi_1 = \phi_2$ points where ϕ_1 and ϕ_2 lie between 180° and 360° correspond to various conformations with the enantiomeric molecular chirality, not all are predicted to exhibit the expected (–)-exciton chirality CD. Some are predicted to show the unexpected (+)-exciton chirality CD.

The probability of encountering conformations that would exhibit the "unexpected" exciton chirality CD behavior may be evaluated from the corresponding conformational potential

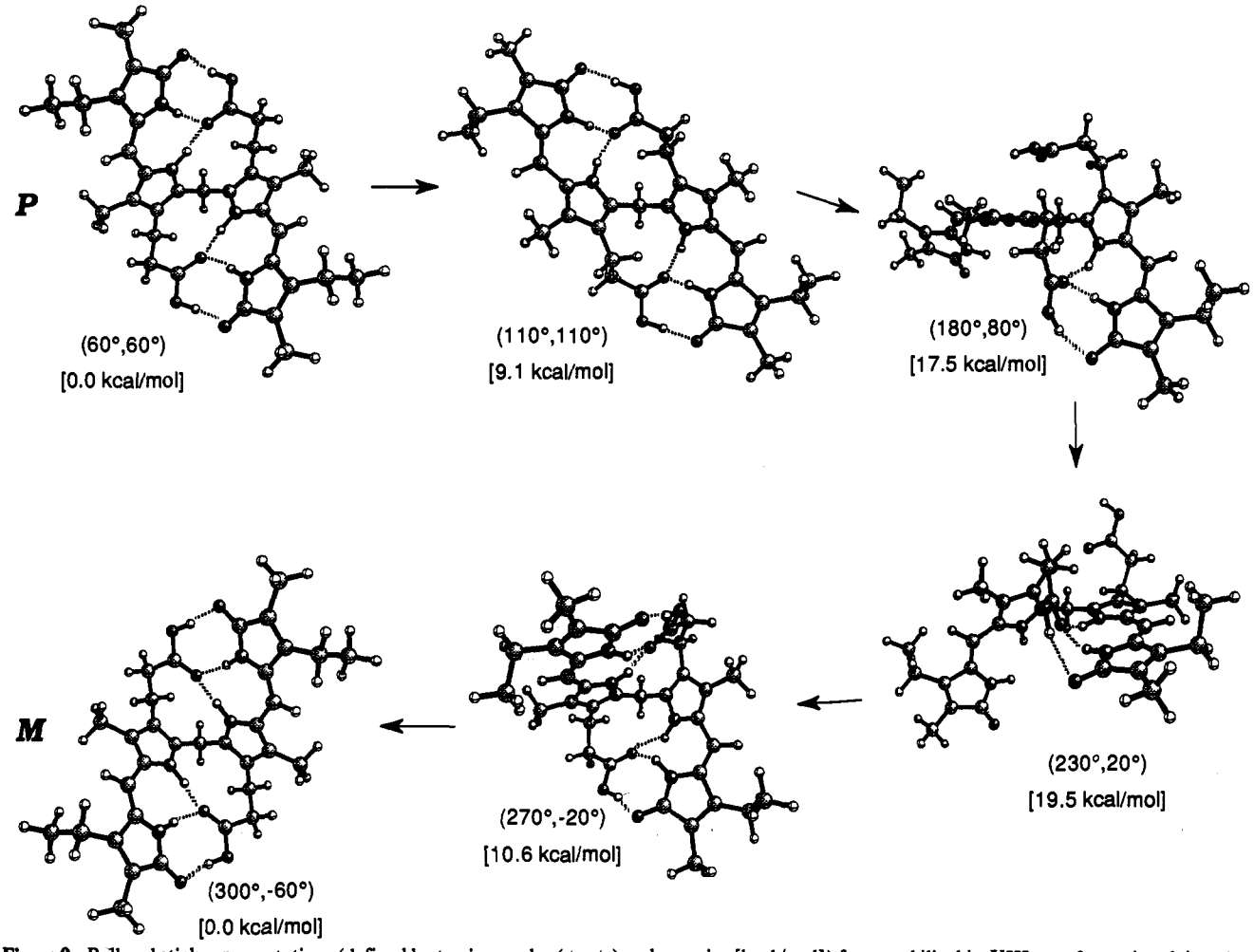

Figure 9. Ball and stick representations (defined by torsion angles (ϕ_1, ϕ_2) and energies [kcal/mol]) for mesobilirubin-XIIIα conformations lying along the lowest energy path (A, Figure 7) for the interconversion of the *P* and *M* chirality global energy minimum enantiomeric conformers. The conformation ($\phi_1 \simeq +230°$, $\phi_2 \simeq +20°$) at the transition state for the interconversion lies some 19.5 kcal/mol above the global minima.

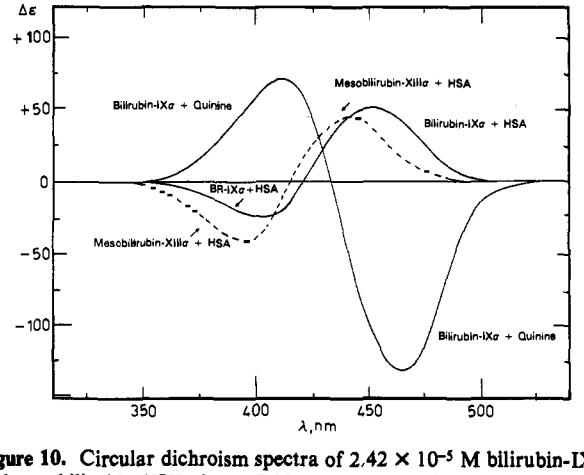

Figure 10. Circular dichroism spectra of 2.42×10^{-5} M bilirubin-IXα and mesobilirubin-XIIIα in pH 7.33 argon-saturated 0.05 M Tris buffer in the presence of 5.07×10^{-5} M human serum albumin at 22 °C; and the circular dichroism spectra of 3.0×10^{-5} M bilirubin-IXα in dichloromethane in the presence of 9.0×10^{-3} M quinine at 21 °C. The CD spectra of the pigments in the absence of amine or protein fall on the $\Delta\epsilon = 0$ line. Neither the protein nor the amine show circular dichroism between 350 and 550 nm.

energies, which are also coplotted in Figure 14 (along the same diagonal). They show that the "inverted" type CD may expected mainly from high-energy ($\phi_1 = \phi_2$) conformations. Ball and stick drawings of representative conformations where $\phi_1 = \phi_2$ may be seen in Figure 15 for structures taken from points along the grey (potential energy) line of Figure 14. In Figure 15, as ϕ_1 and ϕ_2 increase in conrotatory fashion from $\phi_1 = \phi_2 \simeq 0°$, (i) the conformation relaxes from a very high-energy, nearly planar porphyrin-like structure and (ii) passes through lower energy *P*-helical [($\phi_1 = \phi_2 \simeq 20°$) and ($\phi_1 = \phi_2 \simeq 40°$)] conformations where intramolecular hydrogen bonding can be accessed and (iii) on to the *P*-molecular chirality ridge-tile structure ($\phi_1 = \phi_2 \simeq 60°$) lying at a global minimum. (iv) Further rotations about ϕ_1 and ϕ_2 increase the potential energy of the molecule allowing the pigment structure to pass through the gabled conformation ($\phi_1 = \phi_2 = 90°$) and (v) into a series of stretched conformations: one lying near a local minimum at $\phi_1 = \phi_2 \simeq 110°$ and other more stretched conformations lying near $\phi_1 = \phi_2 = 120°$, $\phi_1 = \phi_2 \simeq 140°$, and $\phi_1 = \phi_2 \simeq 160$ where weakened residual hydrogen bonding is accommodated by twisting within the dipyrrinone chromophores that yield large increases in potential energy. The linear conformation ($\phi_1 = \phi_2 \simeq 180°$) lies at an energy maximum. Large $+\Delta\epsilon$ values are predicted for folded helical and ridge-tile conformations, but the magnitude of $\Delta\epsilon$ is expected to decrease as the ridge-tile conformer begins to unfold and stretch into higher energy conformations, dropping to zero at a conformation ($\phi_1 = \phi_2 \simeq 120°$) lying very near the local minimum and lying some 9 kcal/mol above the global minimum. Then with increased unfolding and much higher conformational energies, $\Delta\epsilon$ becomes increasingly negative—before declining rapidly to $\Delta\epsilon = 0$ in the linear conformation ($\phi_1 = \phi_2 \simeq 180°$). At no point along the diagonal path between $\phi_1 = \phi_2 = 0°$ and $\phi_1 = \phi_2 = 180°$, however, does the molecular chirality (*P*?) of the pigment invert.

Inversion of CD Cotton effects ($\Delta\epsilon$) without an accompanying

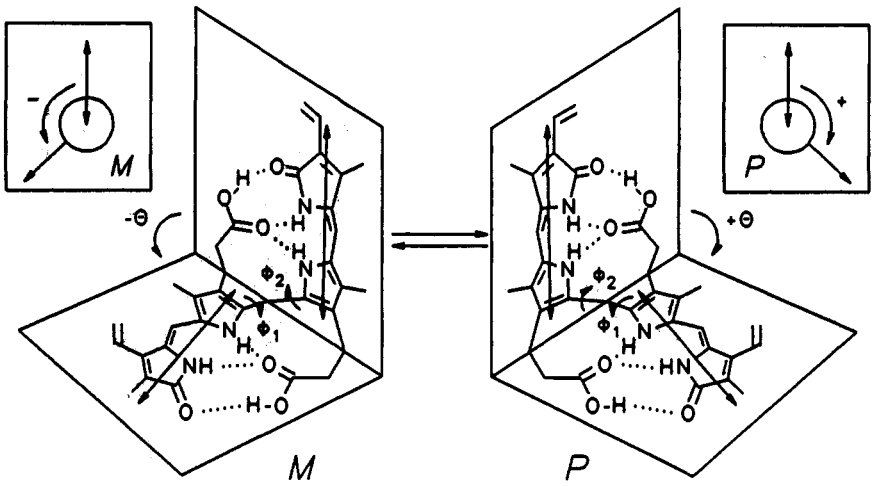

Figure 11. Ridge-tile shaped, folded intramolecularly hydrogen-bonded enantiomeric conformations of bilirubin (*M* and *P*). Interconversion (*M* ⇄ *P*) is accomplished as illustrated in Figures 7 and 8 by rotating about ϕ_1 and ϕ_2. In *M* and *P*, the dipyrrinone chromophores are planar, and the angle of intersection of the two planes (dihedral angle, θ) is ~100° for $\phi_1 \simeq \phi_2 \simeq 60°$. The double-headed arrows represent the approximate direction and intensity of the dipyrrinone long wavelength electric transition dipole moments. The relative orientations or helicities (*M*, minus; *P*, plus) of the vectors are shown (inset) for each enantiomer. For these conformations the *M* dipole helicity correlates with the *M* molecular chirality and the *P* helicity with the *P* molecular chirality.

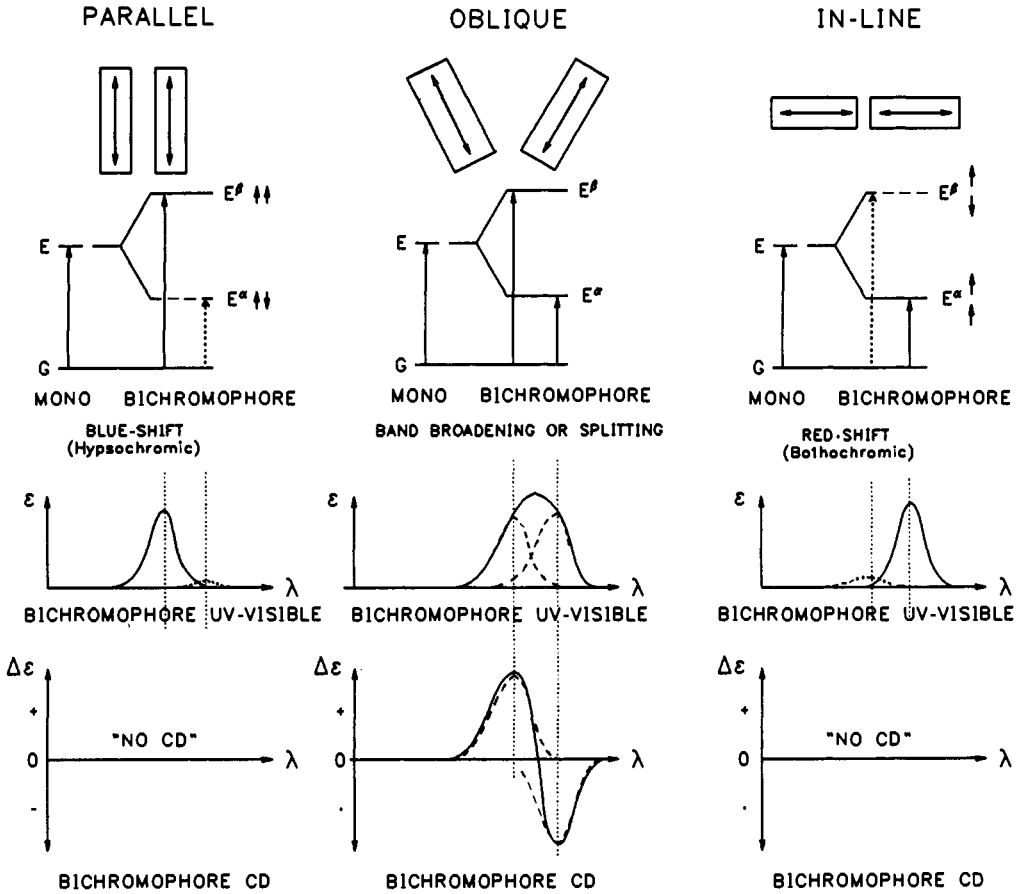

Figure 12. Exciton splitting diagrams (upper) and predicted UV–visible and CD spectra (lower) for the three "limiting" case geometrical arrangements of the electric transition moments: parallel, oblique (of which there are many possible), and linear. The parallel case is represented approximately by the porphyrin-like conformation and the in-line, very approximately by the extended conformation of bilirubin (Figure 4). The oblique case is found in a vast array of folded or helical conformations most notably in the *M* and *P* ridge-tile conformations (Figures 6 and 11) corresponding to the global energy minima. The consequences of the three differing alignments of the electric transition dipoles in the bichromophore may be seen in the differing UV–visible and CD spectra. An arbitrary signed order for the CD couplet is shown. According to exciton chirality theory a bisignate CD with the long wavelength negative–short wavelength positive Cotton effects shown here would indicate a left handed or *M*-helical orientation of the transition dipoles. And a long wavelength positive–short wavelength bisignate CD couplet corresponds to a *P*-helical orientation. Examples of actual bisignate CD spectra may be found in Figure 10.

inversion of molecular chirality occurs because the relative orientation of the dipyrrinone electric transition dipoles invert their relative helicity as the pigment stretches or unfolds (Figure 16) into a broad realm of conformers lying in regions close to and on either side of a diagonal line (Figure 13) connecting points $\phi_1 = 360°$, $\phi_2 = 0°$ and $\phi_1 = 0°$, $\phi_2 = 360°$ and bordered roughly by parallel lines connecting points $\phi_1 = 180°$, $\phi_2 = 0°$ and $\phi_1 = 0°$, $\phi_2 = 180°$, and points $\phi_1 = 360°$, $\phi_2 = 180°$ and $\phi_1 = 180°$,

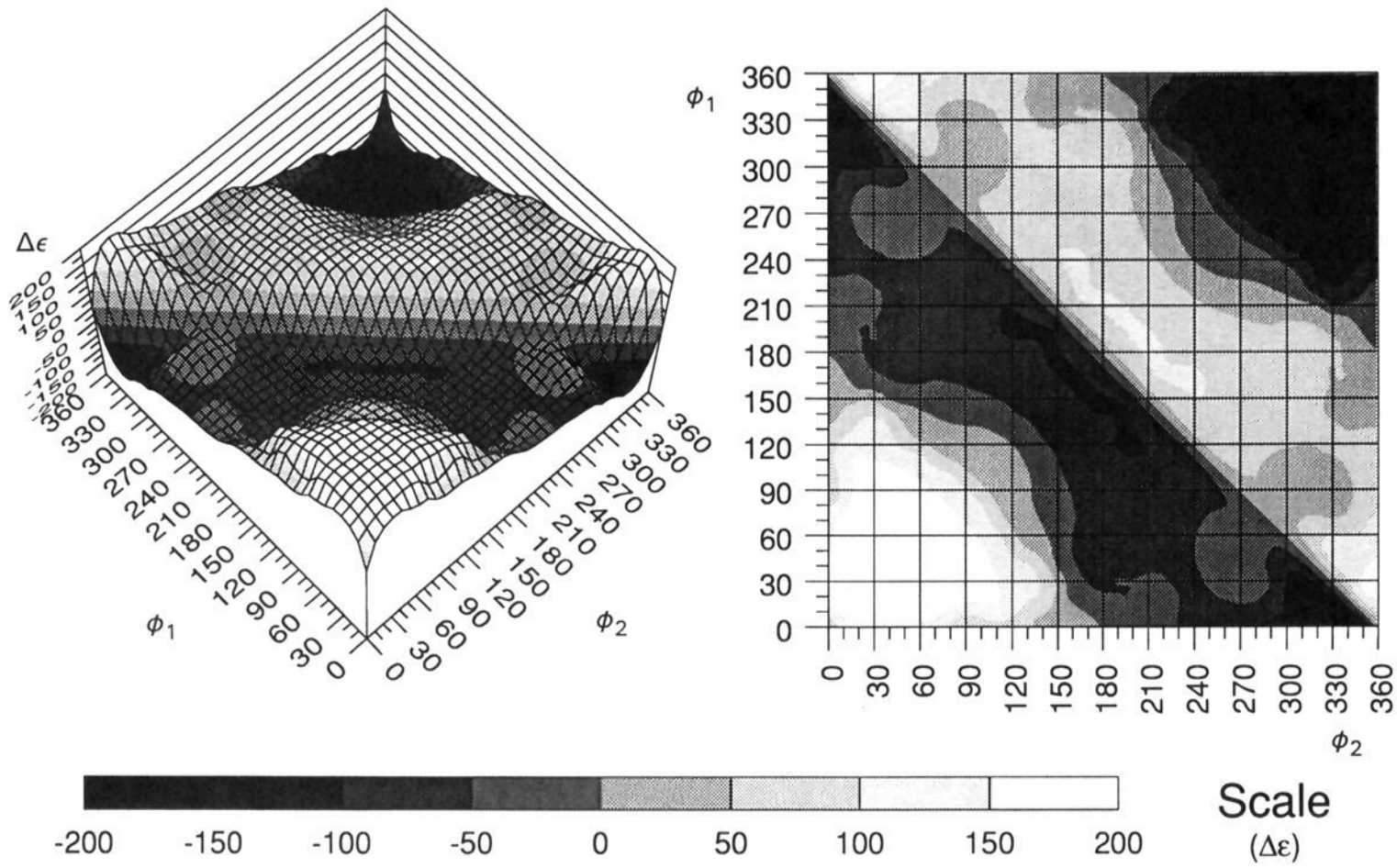

Figure 13. Three-dimensional plot (left) and "topo" map of the variation of computed circular dichroism $\Delta\epsilon$ sign and unscaled magnitude for the lower energy exciton component (α-state) correlated with mesobilirubin and conformations described by independent rotations about torsion angles ϕ_1 and ϕ_2 (Figure 4) from 0 to 360° in steps of 10°. An essentially identical map would be computed for bilirubin-IXα. The diagonal line connects points ($\phi_1 = 0°$, $\phi_2 = 360°$) and ($\phi_1 = 360°$, $\phi_2 = 0°$) separates mirror image conformers (enantiomers), and therefore the sign of $\Delta\epsilon$ (but not its magnitude) corresponding to a given set of (ϕ_1, ϕ_2) coordinates (pigment conformation) becomes inverted by reflection across that diagonal.

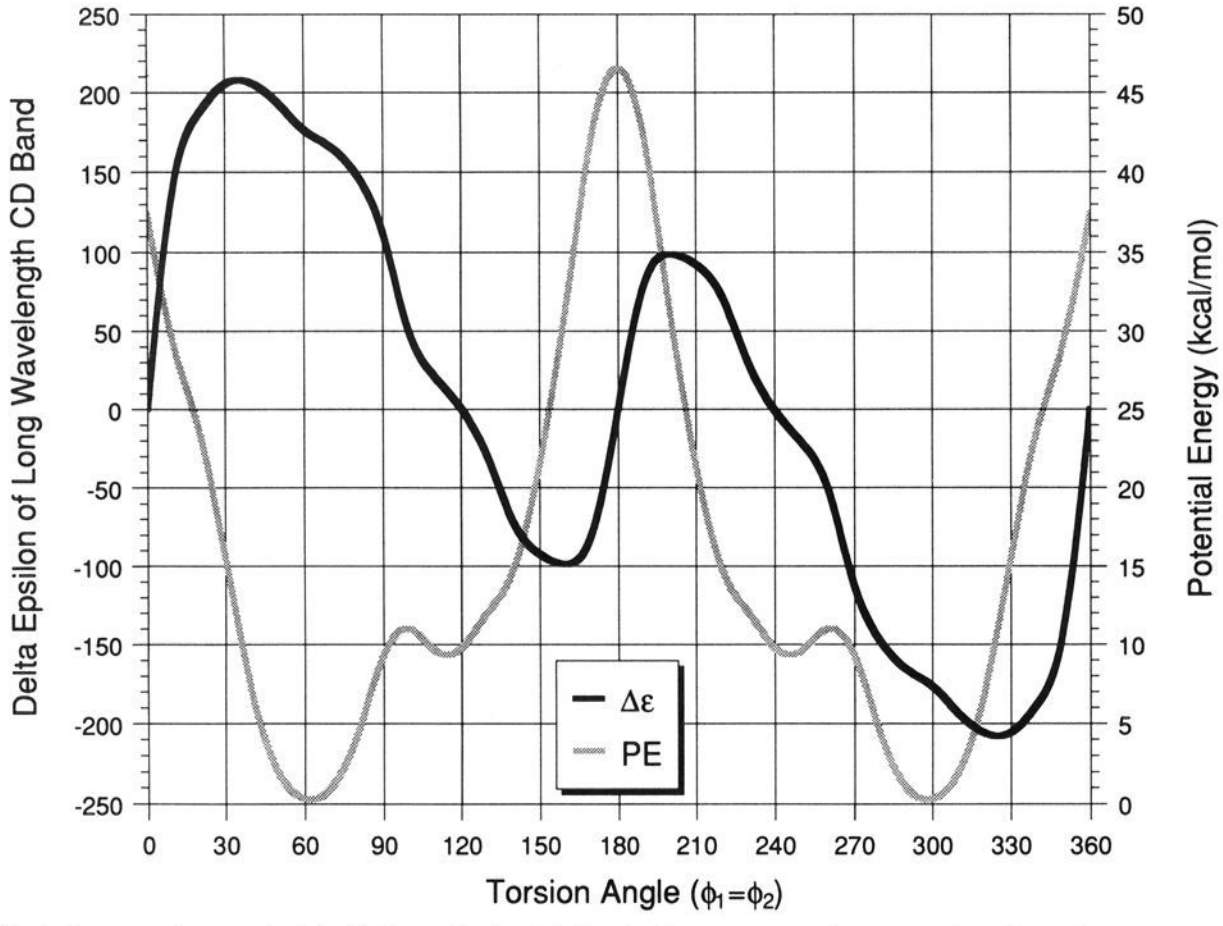

Figure 14. (Black line) Computed, unscaled $\Delta\epsilon$ (left vertical axis) for the lower energy, long wavelength exciton state and its variation with torsion angles ϕ_1 and ϕ_2 along the diagonal (of Figure 13) stretching from ($\phi_1 = \phi_2 = 0°$) to ($\phi_1 = \phi_2 = 360°$). (Grey line) Variation of conformational energy (right vertical axis)—taken from Figures 5 or 7—along the same diagonal for bilirubin-IXα or mesobilirubin-XIIIα.

$\phi_2 = 360°$. Thus, bond rotations about ϕ_1 and ϕ_2, as described by Figures 14 and 15, are predicted to lead to inversion of Cotton effect signs accompanied either with or without inversion of molecular chirality.

In contrast, conformational changes along a slice of the conformational energy maps of Figures 5 and 7, where ϕ_2 is held at 0° and ϕ_1 is rotated from 0° to 180°, lead to inversion of Cotton effect signs only with an inversion of molecular chirality. The computed conformation energies along with the computed CD $\Delta\epsilon$ values (taken from the left edge of Figure 13) for the long wavelength component of the bisignate Cotton effects are plotted in Figure 17. Representative conformations lying at various points ($\phi_2 = 0$, $\phi_1 = 0°$ to 180°) along the curves of Figure 17 are shown in Figure 18. The borders represent special cases, however, and in the more general case, inversion of Cotton effect signs may occur in absence of inversion of molecular chirality to form enantiomers.

Selected computed data (Tables II and III) illustrate the

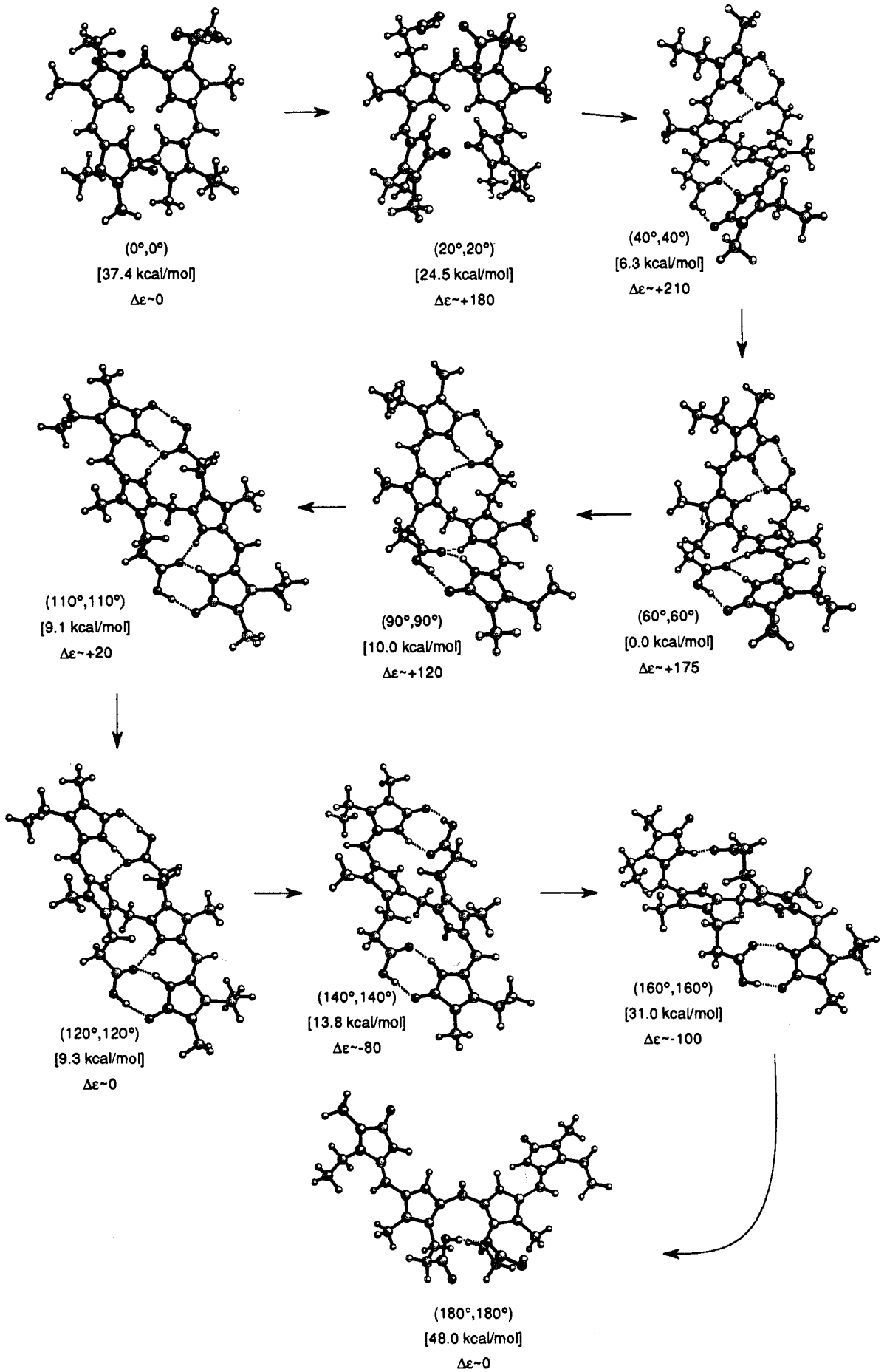

Figure 15. Representative conformations in ball and stick representation for points ($\phi_1 = \phi_2$) lying between 0° and 180° on the conformational potential energy curve of Figure 14.

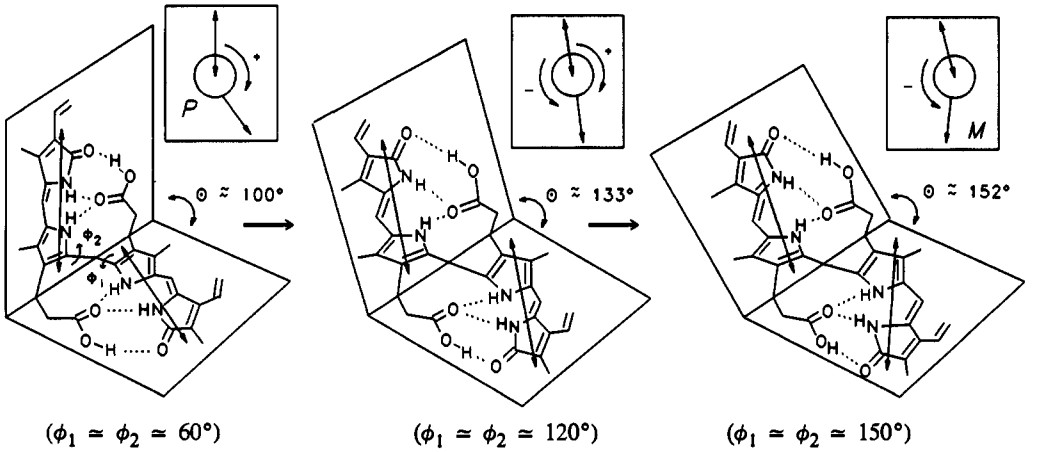

Figure 16. (Left) *P*-Chirality bilirubin in its most stable (global energy minimum) intramolecularly hydrogen-bonded ridge-tile conformation. The intersection of the two dipyrrinone planes makes a dihedral angle, $\theta \simeq 100°$ for torsion angles $\phi_1 = \phi_2 \simeq 60°$ relative to the planar porphyrin-like conformation where ϕ_1 and ϕ_2 are defined as 0°. This conformation is predicted to show a *positive* $\Delta\epsilon$ for the low-energy, long wavelength CD exciton state. (Middle) Stretched *P*-chirality bilirubin arising from rotations about torsion angles ϕ_1 and ϕ_2 to values $\phi_1 = \phi_2 \simeq 120°$ (Figure 14). At or near this conformation, the pigment is predicted to exhibit "no CD" because $\Delta\epsilon$ is computed to be zero. This conformation lies some 10 kcal/mol above the global minimum. (Right) The same conformation and absolute configuration for an even more stretched bilirubin with larger θ and a flatter ridge tile shape. Here $\phi_1 = \phi_2 \simeq 150°$ and in this conformation the pigment is predicted to exhibit a *negative* CD Cotton effect for the low-energy, long wavelength exciton state—in inversion of $\Delta\epsilon$ sign compared with that predicted for the conformation at the far left. This conformation lies some 22 kcal/mol above the global minimum. Conformational stretching is accommodated by lengthening (or breaking) hydrogen bonds between the carboxylic acid CO_2H and lactam –NHC=O groups and by twisting within the individual dipyrrinone chromophores. Consequently, the planes shown in the middle and right structures are only average planes passing through the dipyrrinones. Significantly, the transition dipole vectors, shown in inset boxes, associated with the dipyrrinone long wavelength UV–visible absorption reverse relative orientation from *P* to *M* without an inversion of molecular chirality.

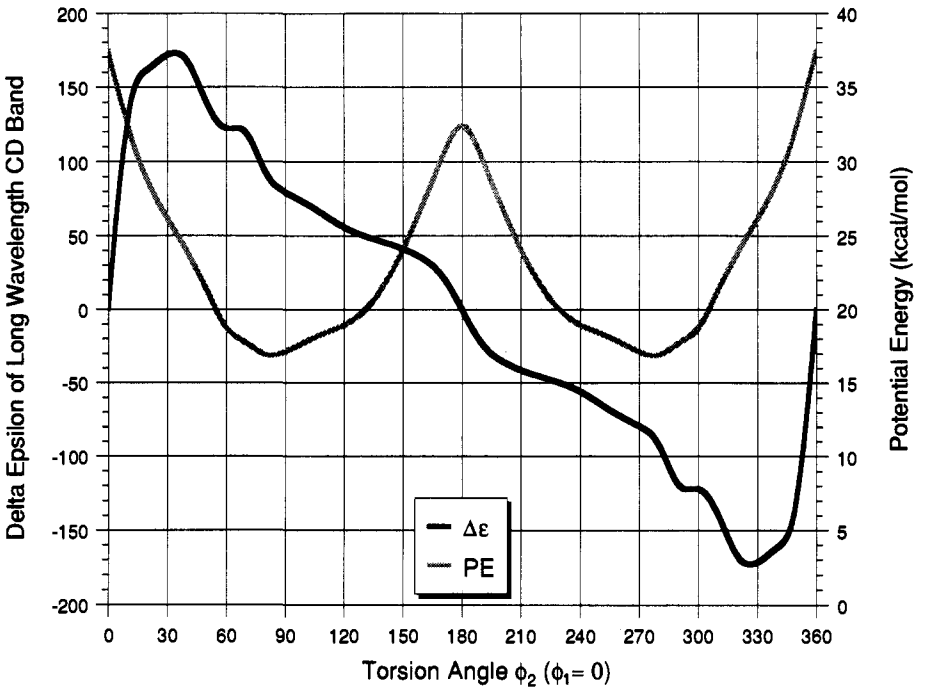

Figure 17. (Black line) Variation of computed $\Delta\epsilon$ (left vertical axis) with torsion angle ϕ_2 (from $\phi_2 = 0°$ to $\phi_2 = 360°$), where ϕ_1 is held at 0°. (Grey line) Variation of conformational energy (right vertical axis)—taken from Figures 5 or 7—along the edge ($\phi_1 = 0°$, $\phi_2 = 0° \rightarrow 360°$) of the conformational energy map for bilirubin-IXα or mesobilirubin-XIIIα.

concepts and principles discussed above. In Table II, which tracks the pathways and conformation illustrated in Figures 17 and 18, the computed UV–visible transitions show the expected (i) blue shift for the porphyrin-like conformations, with parallel transition dipole moments, and (ii) red shift for the extended in-line conformations, with in-line transition dipole moments. The CD Cotton effect $\Delta\epsilon$ values are predicted to reach their largest values for the helical folded conformations and decline to zero in the planar porphyrin-like and the extended in-line conformations. Of course, all of the conformations of Table II are predicted to lie significantly above the global energy minimum ridge-tile conformation, and they are therefore unlikely to be easily accessible.

Computed CD and UV–visible spectra for the *P*-molecular chirality, ridge-tile conformation are shown in Table III, which tracks the pathway and conformations illustrated in Figures 14 and 15. Again, $\Delta\epsilon$ assumes maximum values for helical and folded conformations, including the ridge-tile global minimum conformation. As the ridge-tile conformation begins to stretch through rotations about ϕ_1 and ϕ_2, the magnitude of $\Delta\epsilon$ is predicted

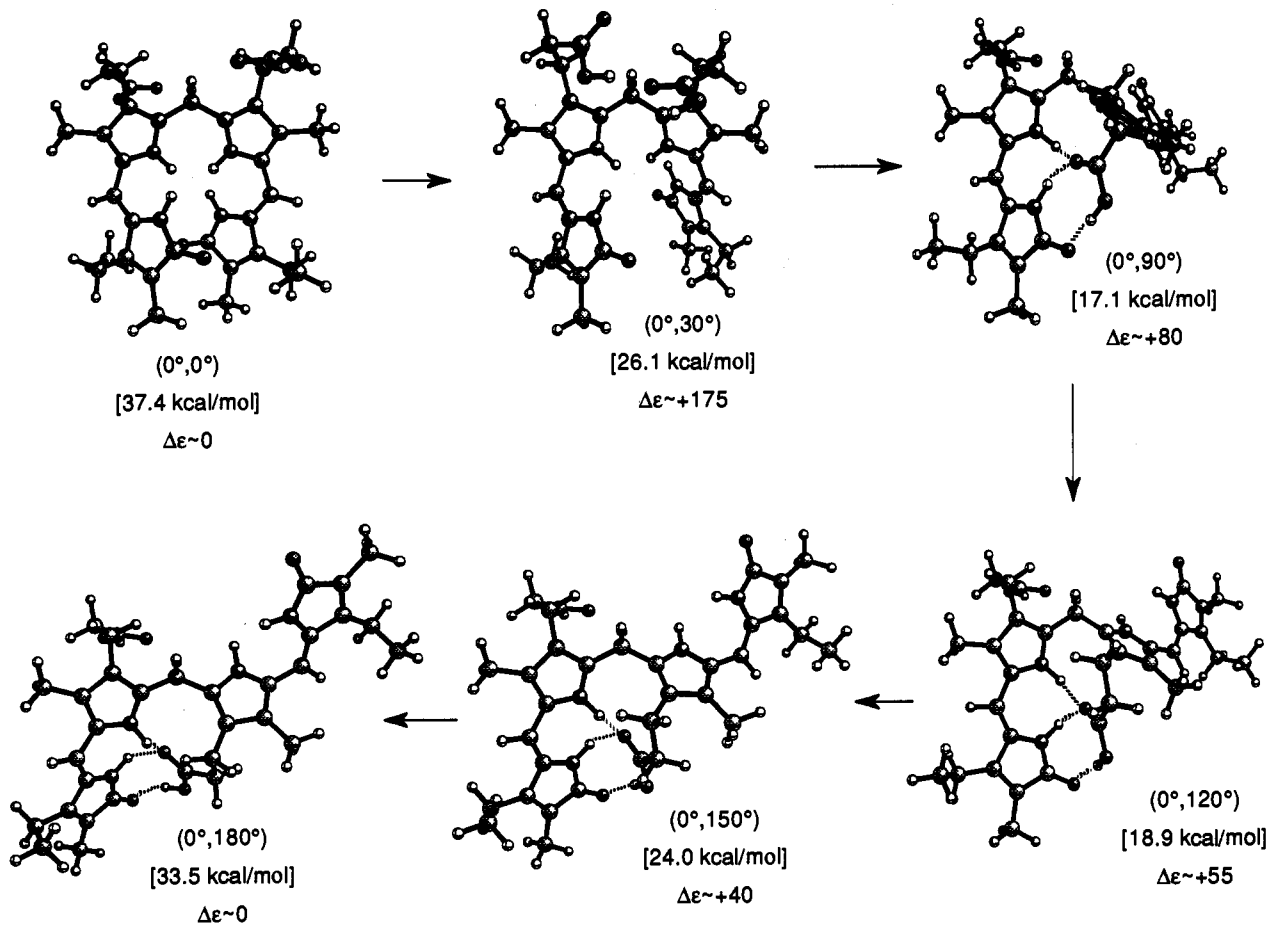

Figure 18. Representative conformations in ball and stick representation for points (ϕ_1, ϕ_2) lying between $\phi_1 = 0°$ and $0° < \phi_2 < 180°$ on the conformational potential energy curve of Figure 17.

Table II. Selected Computed CD and UV–Visible Data[a,b] for Mesobilirubin-XIIIα Conformers: Porphyrin-Like, Helical, Folded, Ridge-Tile Gabled, Stretched, and Extended In-Line (Figure 18) for Selected Points on the Curves of Figures 7 and 16

torsion angle (deg)		conformation	potential energy above	theor UV–visible[c]				summed theor UV–visible		computed CD[c]		
ϕ_1	ϕ_2	type	global min (kcal/mol)	λ^β	ϵ_{max}	λ^α	ϵ_{max}	λ_{max}	ϵ_{max}	λ_1	λ_2	$\Delta\epsilon$ at λ_2
~0	~0	porphyrin-like	37	367	74 000	507	1 000	367	74 000	352	479	~0
0	20	helical	32	402	65 000	454	10 000	403	68 000	378	438	+160
0	30	helical folded	26	403	61 000	450	14 000	406	65 000	378	438	+175
0	60	folded	18	414	42 000	438	34 000	425	70 000	381	434	+120
0	90	gabled	17	418	27 000	434	48 000	428	73 000	381	434	+80
0	100	stretched	18	419	23 000	434	53 000	429	73 000	381	434	+75
0	120	stretched	19	420	14 000	433	61 000	430	74 000	382	434	+55
0	140	stretched	21	419	9 000	433	67 000	431	75 000	382	434	+45
0	160	stretched	27	418	4 000	434	71 000	433	75 000	381	434	+35
0	~180	extended in-line	33	418	1 000	434	74 000	434	75 000	381	434	~0

[a] Based on conformations in which the porphyrin-like conformation passes through *P*-molecular chirality (Figure 18) on the way to extended in-line. [b] ϵ and $\Delta\epsilon$ in M/cm. [c] For the β-state and α-state of the molecular exciton. [d] Folded, with intramolecular hydrogen bonding.

to decrease substantially as the local minimum conformation is approached. In a stretched conformation ($\phi_1 = \phi_2 \simeq 120°$), $\Delta\epsilon$ is predicted to be ~0; then, with further stretching by rotation about ϕ_1 and ϕ_2, the sign of $\Delta\epsilon$ reverses. Reasonably large reversed-sign $\Delta\epsilon$ values are found in high-energy stretched conformations near $\phi_1 = \phi_2 \simeq 140°$ and $\phi_1 = \phi_2 \simeq 160°$. In the planar linear conformation, $\Delta\epsilon = 0$.

As indicated in Tables II and III, in going from the gabled or the ridge-tile conformation to the planar porphyrin-like conformation (where $\Delta\epsilon = 0$), the "observed" UV–visible maximum is computed to shift toward the blue, to shorter wavelengths as the relevant transition dipoles move toward a parallel aligment (Figure 12). On the other hand, as the ridge-tile or the gabled conformation of Table III is stretched, the "observed" UV–visible maximum is predicted to red-shift, until the conformation approached $\phi_1 = \phi_2 \simeq 120°$, where the relevant dipyrrinone transition dipoles adopt an on-line orientation. The CD $\Delta\epsilon$ is predicted to be zero here. With further stretching, the "observed" UV–visible maximum shifts toward the blue due to a realignment of the transition moments. In contrast, as the gabled conformation of Table I stretches into the extended in-line, the "observed" UV–visible maximum is computed to shift toward the red as the relevant transition dipoles move 180° apart—as in the in-line arrangement of Figure 12. Thus for mesobilirubin-XIIIα, the porphyrin-like conformation is predicted to have the shortest wavelength UV–visible absorption (~367 nm) with the narrowest band width. The global minimum stretched (Table III) and high-energy extended in-line (Table I) conformations are predicted to have the longest wavelength UV–visible absorption (~435 nm) with the narrowest band width. And the global minimum ridge-tile conformation is predicted to have a broad UV–visible absorption at an intermediate maximum wavelength (427 nm).

Table III. Selected Computed Circular Dichroism and UV–Visible Data[a,b] for Mesobilirubin-XIIIα Conformers: Porphyrin-Like, Helical, Folded, Ridge-Tile, Gabled Stretched, and Linear (Figure 15) for Selected Points on the Curves of Figures 7 and 14

torsion angle (deg)		conformation	potential energy above	theoretical UV–visible[c]				summed theor UV–visible		computed CD[c]		
ϕ_1	ϕ_2	type	global min (kcal/mol)	λ^β	ϵ_{max}	λ^α	ϵ_{max}	λ_{max}	ϵ_{max}	λ_1	λ_2	$\Delta\epsilon$ at λ_2
~0	~0	porphyrin-like	37	367	74 000	507	1 000	367	74 000	352	479	~0
20	20	helical	24	405	58 000	450	17 000	409	64 000	379	438	+190
40	40	helical folded	6	402	44 000	453	31 000	414	54 000	378	438	+210
60	60	ridge-tile[d] (global min)	0	407	36 000	446	40 000	427	55 000	401	437	+175
90	90	gabled	10	411	25 000	442	50 000	433	67 000	380	435	+120
110	110	local min	9	405	30 000	450	45 000	435	58 000	379	438	+20
120	120	stretched	9	404	34 000	451	41 000	433	54 000	378	438	~0
140	140	stretched	14	399	45 000	456	30 000	406	51 000	377	440	–80
160	160	stretched	31	401	50 000	454	25 000	406	56 000	378	439	–100
~180	~180	linear	48	408	73 000	446	73 000	409	74 000	380	436	~0

[a] Based on conformations in which the porphyrin-like conformation passes through *P*-molecular chirality (Figure 15) on the way to linear. [b] ϵ and $\Delta\epsilon$ in M/cm. [c] For the β-state and α-state of the molecular exciton. [d] With intramolecular hydrogen bonding.

The last is, in fact, typically observed in solutions of mesobilirubin in organic solvents[16,33] and in pH 7.4 aqueous buffer.[39] Qualitatively similar UV–visible and CD spectral characteristics are predicted for bilirubin-IXα—except with all wavelength red-shifted by ~25 nm due to the presence of vinyl groups located on the lactam rings.

Configurational Assignment of Bilirubin Conformers. A graph of nonplanar (helical) conformations of bilirubin follows from the diarylmethane conformational analysis of Gust and Mislow[44] and Falk's analyses of dipyrrylmethane conformations.[23] Using the central dipyrrylmethane unit (Figure 4B) of bilirubin or mesobilirubin as abbreviated forms, the entire range of chiral conformations and their interconversions (shown in Figure 20) can be designated according to standard stereochemical nomenclature:[23] *sc* and *ac*. The related planar conformations of Figure 4 carry the designations *sp* and *ap*. The *M*-molecular chirality pigment of Figures 6, 8, 9, and 11 is found at the *–sc*, *–sc* vertex, and its *P*-molecular chirality enantiomer at the *+sc*, *+sc* vertex. The corners of the cube correspond to the four *d,l* enantiomeric pairs of helical conformations of unsymmetrically substituted bilirubins and mesobilirubins. But for the symmetrically substituted isomers, *e.g.*, mesobilirubin-XIIIα, the pairs of enantiomers *+ac*, –sc, –ac, +sc and +sc, *–ac*, *–sc*, *+ac* are equivalent. In Figure 20, conformations joined by dashed lines through the center of the cube are enantiomeric. Interconversions of enantiomers by the dashed line routes involve synchronous rotations about ϕ_1 and ϕ_2, passing through a planar geometry. For example, interconversion of the *–sc*, *–sc* and *+sc*, *+sc* enantiomers along the dashed line passes through the planar, porphyrin-like conformation (*sp*, *sp*) shown in Figure 4. The *–ac*, *–ac* and *+ac*, *+ac* pair are related by passing through the planar, linear conformation (*ap*, *ap*) of Figure 4. And the two pairs *+ac*, *–sc*, *–ac*, *+sc* and *+sc*, *–ac*, *–sc*, *+ac* interconvert through either of two planar, extended conformations *ap*, *sp* or *sp*, *ac*. However, since the planar conformations represent energy maxima (peaks) on the conformational energy surfaces of bilirubin or mesobilirubin (Figures 5 and 7), all of the interconversion pathways cited above are predicted to be very high energy and thus unlikely.

The lowest energy interconversion pathways for the enantiomeric pairs follow the edges of the cube of Figure 20. This can be seen for the interconversion of *+sc*, *+sc* to *–sc*, *–sc*, which may pass initially either through *+ac*, *–sc*, *–sc*, *+ac* or *+ac*, *+ac*, the three adjacent vertices or conformations as the cube. In point of fact, as explained on the basis of an analysis of the conformational energy map of mesobilirubin-XIIIα, path A (Figures 7 and 9), which takes the *P*-helical conformation at point $\phi_1 = \phi_2 = 60°$, which corresponds to *+sc*, *+sc*, through the conformational point $\phi_1 = \phi_2 = 110°$, corresponding to *+ac*, *+ac* and then through the conformational point $\phi_1 = 230°$, $\phi_2 = 20°$, corresponding to *–ac*, *+sc*, before going to the *M*-helical enantiomeric conformation at point $\phi_1 = 300°$, $\phi_2 = -60°$, corresponding to *–sc*, *–sc*.

The chirality of the helical conformations can be described with reference to a (i) *plane of chirality* (determined by C_9, C_{10}, and C_{11}) and the distribution of N_{22} and N_{23} nitrogen reference points on the two sides of the plane of chirality and (ii) an *axis of chirality* (determined by a line perpendicular to the plane of chirality and passing through C_{10}). The sense of twist of the molecular propellar (propeller chirality) may be that of either a left- or a right-handed helix, denoted by a (–) or a (+), respectively, at each vertex of the cube of Figure 20.[40] However, as indicated earlier, the helicity of the propeller does not always correspond to the helicity of the dipyrrinone induced electric dipole transition moments in the exciton chirality analysis.

Correlation of Exciton Circular Dichroism With Absolute Configuration. Exciton chirality theory allows for the prediction of the absolute configuration of a bichromophore molecule such as bilirubin if the relative orientation of the relevant electric transition dipole moments are known.[17] A typical exciton coupling-type CD curve is bisignate (Figure 10). Enantiomers have mirror image CD curves—either a curve with a long wavelength positive–short wavelength negative or a curve with long wavelength negative–short wavelength positive series of Cotton effects. Thus, the two exciton states (UV–visible transitions) predicted in Figure 12 for the oblique case (the other two cases predict zero CD) each give rise to two corresponding CD transitions, which are always oppositely signed.[17] The two possible signed sequences of Cotton effects can be correlated with the relative orientation of the transition dipoles. When the dipoles are oriented with a positive (+) torsion angle, corresponding to a positive helicity, the sequence of Cotton effect signs in the CD is long wavelength positive–short wavelength negative. When the torsion angle is negative (–), corresponding to a negative helicity, the sequence is long wavelength negative–short wavelength positive—as illustrated in Figure 12. The latter orientation clearly corresponds to the *M*-molecular chirality global minimum ridge-tile conformer of Figure 11; the former corresponds to the *P*-molecular chirality of Figure 11.

Unfortunately, according to the analysis of the preceding section, a *P*-molecular chirality conformation can also exhibit a negative chirality bisignate CD—simply by rotating about ϕ_1 and ϕ_2 so as to access conformations without changing the molecular chirality but with a reversed helicity of the dipyrrinone

(39) Lightner, D. A.; Reisinger, M.; Landen, G. L. *J. Biol. Chem.* **1986**, *261*, 6034–6038.
(40) Gust, D.; Mislow, K. *J. Am. Chem. Soc.* **1973**, *95*, 1535–1547.
(41) Boiadjiev, S. E.; Person, R. V.; Lightner, D. A. *J. Am. Chem. Soc.* **1993**, *115*, 10123–10133.
(42) Puzicha, G.; Pu, Y.-M.; Lightner, D. A. *J. Am. Chem. Soc.* **1991**, *113*, 3583–3592.
(43) Deutsche, C. W.; Lightner, D. A.; Woody, R. W.; Moscowitz, A. *Annual Rev. Phys. Chem.* **1969**, *20*, 407–448.
(44) Lightner, D. A.; Reisinger, M.; Wijekoon, W. M. D. *J. Org. Chem.* **1987**, *52*, 5391–5395.

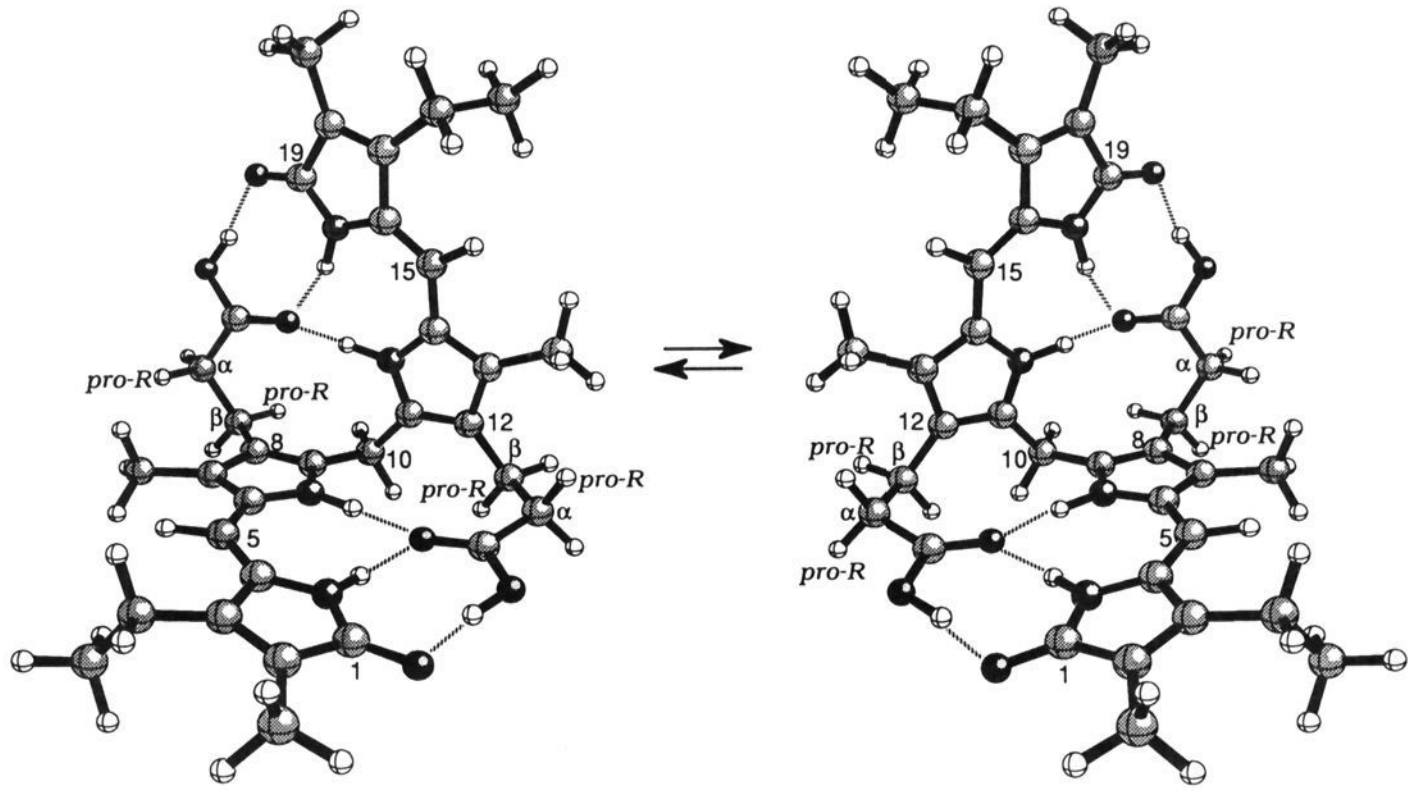

Figure 19. Ball and stick models of folded intramolecularly hydrogen-bonded mesobilirubin-XIIIα. The (*pro-R*) α-hydrogens are sterically compressed into the CH_3 groups at C_7 and C_{13}, and the (pro-*R*) β-hydrogens are sterically crowded by the $-CH_2-$ at C_{10} in the ***M***-helicity conformation. The *pro-S* hydrogens are sterically crowded in the ***P***-helicity conformation. Replacing the *pro-R* hydrogens by CH_3 groups drives the equilibrium toward ***P***, and replacing the *pro-S* by CH_3 groups drives it toward ***M***. However, replacing one *pro-R* and one *pro-S* hydrogen by CH_3 gives a *meso* diastereomer (*R*,*S*) that can adopt either the ***M*** or the ***P*** conformation while leaving one propionic acid ineffectively hydrogen bonded.

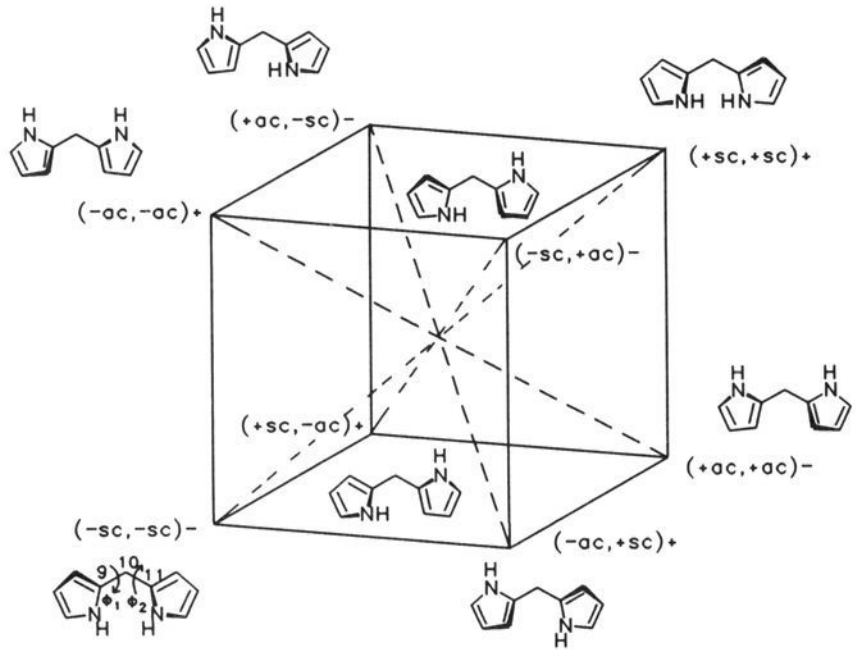

Figure 20. Interconversion graph relating the four possible *d*,*l* paris of "helical" propeller conformations and their interconversions for unsymmetrically substituted bilirubins represented for simplicity as the central dipyrrylmethane unit. In symmetrically-substituted bilirubins, *e.g.*, mesobilirubin-XIIIα, there are only three *d*,*l* pairs as the *+sc*, *–ac*, *sc*, *+ac* set becomes identical with the *+ac*, *–sc*, *–ac*, *+sc* set. Each vertex and associated helical conformation is defined in stereochemical nomenclature of Klyne and Prelog. Rotations about ϕ_1 and ϕ_2 interconvert the conformations illustrated on the graph. In addition, each vertex is marked with a symbol + or –. A "+" indicates a positive helical propeller chirality, while "–" denotes a negative helical propeller chirality.

electric transition dipoles (Figure 16). Given this possible ambiguity, it seemed wise to correlate a well-defined chiral conformation of bilirubin with its CD spectrum. This was accomplished experimentally through a forced enantioselection by intramolecular allosteric effects.

Intramolecular Allosteric Effects on Bilirubin Enantioselection. Inspection of CPK space-filled molecular models of bilirubin and mesobilirubin-XIIIα or examination of structure through molecular modeling reveals unique and important stereochemical facets of the intramolecularly hydrogen-bonded enantiomeric conformers (Figures 6 and 11). When the propionic acid carboxyls are linked through intramolecular hydrogen bonding to the opposing dipyrrinones, their $-CH_2CH_2-$ segments are brought into close proximity to the methyls at C_7 and C_{13} and to the methylene group at C_{10}. This is depicted in the ball and stick models of mesobilirubin-XIIIα in Figure 19, which shows that the stereochemical model presented does not depend on the presence of vinyl groups. As illustrated, when the pigment is folded into the ***M***-molecular chirality ridge-tile enantiomer, the (*pro-R*)-β-hydrogen (but not the *pro-S*) is brought into close nonbonded contact with the $-CH_2-$ group at C_{10}. In the ***P***-molecular chirality enantiomer, it is the (pro-*S*)-β-hydrogen that is buttressed against the C_{10} $-CH_2-$ group. Further examination of the ***M***-chirality conformer reveals that the (*pro-R*)-α-hydrogens lie in close proximity to the methyl groups at C_7 and C_{13}, whereas the (*pro-S*)-α-hydrogen lies in an uncongested environment. In the ***P***-molecular chirality enantiomer, it is the (pro-*S*)-α-hydrogens that are buttressed against the methyl at C_7 and C_{13}. Consequently, when mesobilirubin (or bilirubin) adopts either of the thermodynamically preferred enantiomeric ridge-tile conformations (Figures 6, 11, or 19), one conformational enantiomer can be destabilized relative to the other through allosteric action from judiciously placed methyl groups on the propionic acid side chains. For example, insertion of a methyl group at the *pro-R* site on either the β-carbon or α-carbon of the propionic acid would be expected to destabilize the ***M***-molecular chirality intramolecularly hydrogen-bonded conformational enantiomer by introducing a severe nonbonded β-CH_3 to C_{10}-CH_2, or α-CH_3 to C_7- or C_{13}-CH_3 steric interaction (Figure 19). Such steric buttressing would be expected to shift the conformational equilibrium toward ***P***-molecular chirality enantiomer. In contrast, introduction of a methyl group at the *pro-S* sites would destabilize the ***P***-molecular chirality enantiomer and shift the equilibrium toward ***M***. Thus, appropriately inserted methyl groups can be expected to force a resolution of bilirubin into its conformational enantiomers (diastereomers) through the action of intramolecular allosteric effects. This thesis was recently examined and validated by the synthesis of bilirubin analogs (Figure 21), β,β'-dimethylmesobilirubin-XIIIα (**1**)[41] and α,α'-dimethylmesobilirubin-XIIIα (**2**).[42]

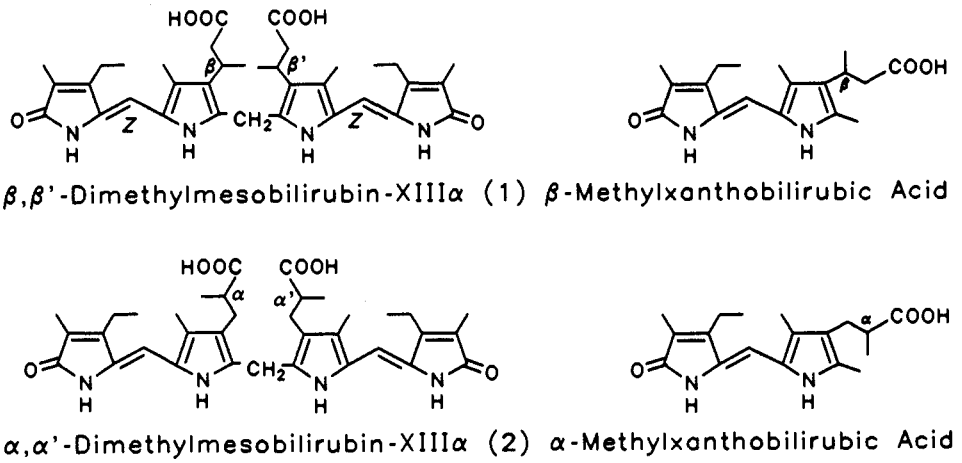

Figure 21. Linear representations for synthetic β,β'- and α,α'-dimethylmesobilirubin-XIIIα diastereomers and their dipyrrinone precursors.

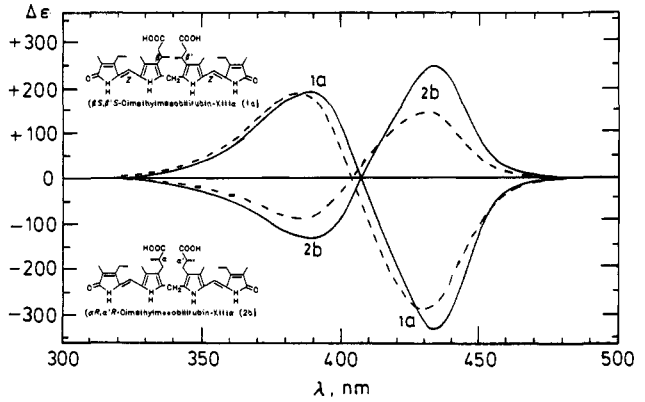

Figure 22. Bisignate circular dichroism spectra of 10^{-5} M ($\beta S,\beta'S$)-dimethylmesobilirubin-XIIIα (**1a**) and ($\alpha R,\alpha'R$)-mesobilirubin-XIIIα (**2b**) in $CHCl_3$ (—) and CH_3OH (– –) solvents at 22 °C.

Thus, stereospecific total syntheses were devised for both the (S,S) and the (R,R) enantiomers of β,β'-dimethylmesobilirubin-XIIIα (**1**) in which enantiomeric resolution and determination of absolute configuration was completed at the monopyrrole stage.[41] In a separate synthesis, a mixture of the (S,S), (R,R), and (R,S) diastereomers of α,α'-dimethymesobilirubin-XIIIα (**2**) was separated chromatographically into *meso* (R,S) and racemic (S,S + R,R) diastereomers, and the latter was resolved using human serum albumin or quinine as resolving agents.[42] Evidence for the predicted allosteric effect on these bichromophore pigments came first from comparing optical rotations. Thus, the bichromophoric ($\beta S,\beta'S$) enantiomer of **1** had an enormously high rotation $[\alpha]^{20}_D$ −5200°, whereas the monochromophoric (βS)-methylxanthobilirubic acid had a much weaker rotation $[\alpha]_D$ +63° (both in $CHCl_3$).

The ($\alpha S,\alpha S'$) enantiomer of **2** had a comparably large $[\alpha]_D$ −5000°, whereas (αS)-methylxanthobilirubic acid had only $[\alpha]_D$ +50° (both in $CHCl_3$). On the basis of the monochromophore rotations, one might have predicted rotations of the bichromophore to be ~ ±100°. However, the enormous rotations actually seen are clear indication of a special type of optical activity not arising merely from the influence of a remote chiral center perturbing (electronically) a dipyrrinone chromophore.[43,44] Analysis of their circular dichroism spectra confirmed the importance of conformational stabilization through intramolecular hydrogen bonding.

Bilirubin Circular Dichroism and Structure. The intense, bisignate CD spectra (Figure 22) seen for the ($\beta S,\beta'S$) and ($\alpha R,\alpha'R$) enantiomers (**1a** and **2b**, respectively) of the dimethyl analogs of mesobilirubin-XIIIα, are consistent with the allosteric model described above. No chiral complexation agents are required for the observed CD, which is due to the intrinsic stereochemistry of the pigment. The ($\beta S,\beta'S$)-methyl groups of **1** are predicted to displace the equilibrium (Figure 19) toward the *M*-molecular chirality conformer, whereas a forced displacement toward the *P*-molecular chirality conformer is predicted from ($\alpha R,\alpha'R$)-methyl substitution in **2**. Indeed, the CD curves shown in Figure 22 are of the mirror image bisignate type. Those solvents which preserve intramolecular hydrogen bonding can be expected to favor large Cotton effects. Thus, nonpolar solvents such as chloroform and tetrahydrofuran show long wavelength $\Delta\epsilon$ values ranging from 225 to 250 M/cm, but even in *polar* aprotic solvents such as acetone and acetonitrile very large $\Delta\epsilon$ values can be found (Table IV). Although large $\Delta\epsilon$ values are found for the ($\beta S,\beta S$)-diastereomer in polar protic solvents such as methanol, the $\Delta\epsilon$ values are much reduced in the CD of α,α'-dimethyl isomer. The reasons for this are not entirely clear. Apparently solvent polarity and solvent hydrogen-bonding forces promote only minor destabilization of the intramolecularly hydrogen-bonded pigment structure in the case of the β,β'-dimethyl isomer but have a greater effect on disrupting intramolecular hydrogen bonding in the α,α'. Attempts to correlate CD and structure with the solvent dielectric constant are not entirely unsatisfactory. With reduced intramolecular hydrogen bonding, or solvent-coordinated hydrogen bonding, the pigment can apparently adopt other conformations more easily, *e.g.*, by (i) rotations of the dipyrrinones about torsion angles ϕ_1 and ϕ_2 and/or (ii) lowering the activation energy for interconversion of the folded (but not necessarily intramolecularly hydrogen-bonded) enantiomeric conformers located at the global energy minima. Both (i) and (ii) would lead to reduced $\Delta\epsilon$ values; however, since the UV–visible spectra do not differ significantly, when the $\Delta\epsilon$ values are reduced, the conformations are predicted by exciton coupling theory to be similar in the organic solvents used. In the aqueous buffer, however, where $\Delta\epsilon$ values are ~50% of those seen in organic solvents and where the pigments (anions) show a 6–12-nm blue shift in the UV–visible spectra, the intrusion of a more folded (Tables I and II) or a stretched (Table II) conformation—possibly facilitated by insertion of solvent molecules in the intramolecular hydrogen bonding matrix—is a possible rationale. A full conformational analysis of bilirubin dicarboxylate anion is currently under study in our laboratory and will be reported separately.

Concluding Comments

The preceding studies of bilirubin conformational analysis and circular dichroism point to a folded ridge-tile conformation as the global energy minimum. Conformational stabilization is due to two factors: (i) minimization of nonbonded steric interactions and (ii) powerful stabilization through intramolecular hydrogen bonding. The importance and relevance of intramolecular hydrogen bonding in bilirubins and their strong tendency to implement such hydrogen bonding is underscored by our studies.

Table IV. Circular Dichroism and UV–Visible Spectral Data for 1.3×10^{-5} M Solutions of ($\beta S,\beta' S$)- and ($\alpha R,\alpha' R$)-Dimethylmesobilirubin-XIIIα at 22 °C

			CD[b]			
enantiomer	solvent	dielectric constant[a]	$\Delta\epsilon_{max}$ (λ_1)	λ_2 at $\Delta\epsilon = 0$	$\Delta\epsilon_{max}$ (λ_3)	ϵ_{max} λ(nm)
($\beta S,\beta' S$)-1	chloroform	4.7	+186 (389)	407	–337 (434)	55 500 (431)
($\alpha R,\alpha' R$)-2			–123 (393)	408	+246 (436)	56 000 (433)
($\beta S,\beta' S$)-1	tetrahydrofuran	7.3	+188 (390)	406	–338 (433)	56 200 (431)
($\alpha R,\alpha' R$)-2			–128 (391)	407	+226 (434)	52 000 (432)
($\beta S,\beta' S$)-1	acetone	20.7	+182 (387)	404	–322 (430)	55 400 (426)
($\alpha R,\alpha' R$)-2			–125 (388)	405	+226 (432)	55 600 (426)
($\beta S,\beta' S$)-1	acetonitrile	36.2	+181 (384)	403	–315 (429)	55 000 (423)
($\alpha R,\alpha' R$)-2			–121 (386)	403	+214 (429)	55 200 (425)
($\beta S,\beta' S$)-1	methanol	32.6	+177 (386)	405	–285 (431)	56 600 (425)
($\alpha R,\alpha' R$)-2			–85 (388)	406	+141 (432)	55 700 (426)
($\beta S,\beta' S$)-1	phosphate		+107 (379)	397	–171 (424)	52 000 (418)
($\alpha R,\alpha' R$)-2	buffer, pH 8.5		–84 (379)	399	+117 (425)	52 000 (418)

[a] From Gordon, A. J.; Ford, R. A. *The Chemist's Companion*, Wiley: New York, 1972; pp 4–8. [b] From refs 21 and 22.

Intramolecular hydrogen bonding is, in fact, found to be retained in a wide variety of solvents, and it very likely plays a prominent role in even water at alkaline pH, where the carboxylic acid groups become ionized. The latter evidence is particularly relevant to ongoing studies in aqueous solutions involving protein binding, conjugation, and hepatic excretion of bilirubins. Bilirubin itself can be predicted to be resolvable into its intramolecularly hydrogen-bonded conformational enantiomers if the interconversion barrier is increased and the rate of interconversion retarded, *viz.* at sufficiently low temperatures. Although such a resolution into conformational enantiomers has not yet been achieved, resolution has been accomplished for synthetic analogs where intramolecular steric repulsions render one conformational enantiomer destabilized relative to the other, *e.g.*, through substitution of a propionic acid β-H (or α-H) by CH_3 to give enantiomeric β,β'-dimethylmesobilirubins-XIIIα. The stereospecifically synthesized (*S,S*) and (*R,R*) enantiomers are shown to adopt the *M* and *P* ridge-tile conformations, respectively, which exhibit intense bisignate mirror image CD curves originating from an exciton splitting mechanism. Here, the designations *P* and *M* represent both molecular chirality and the chirality of the component dipyrrinone long wavelength induced electric dipole transition moments according to the exciton model. However, interestingly and perhaps surprisingly, computations have shown that the exciton chirality CD curves can become *inverted without a change in molecular chirality* (for example, the *P*-molecular chirality can give an *M*-helicity bisignate CD curve) simply by stretching or flattening the ridge-tile shape somewhat. However, it must be stressed that the necessary conformational changes are energy-demanding, and those conformers with inverted CD curves are computed to lie much higher in energy than the global minimum. Nonetheless, our studies suggest that previously observed CD spectra with moderate or weak $\Delta\epsilon$ values (as with bilirubin on human serum albumin (Figure 10)) may be attributed to conformational changes as much as to incomplete enantioselection by the chiral complexation agent.

Experimental Section

Bilirubin-IXα (Porphyrin Products) was purified as described previously.[12] Mesobilirubin-XIIIα and its optically active β,β'-dimethyl and α,α'-dimethyl isomers were prepared as reported.[41,42,45] Circular dichroism spectra were run on pH 7.4 aqueous solutions containing human serum albumin[18,39,46] or in organic solvents[16] as described previously.

Conformational energy maps for the molecular modeling of the pigments of this work follow from molecular mechanics calculations carried out on an Evans and Sutherland ESV-10 workstation using version 5.5 of SYBYL (Tripos Assoc., St. Louis, MO) using the following parameters: tripos force field, electrostatics calculated (Gasteiger-Hückel), boundary conditions ignored. Molecular mechanics were run using the maximin2 routine with the following parameters: LS_ACCURACY = 0.001, LS_STEP_SIZE = 0.001, MAX_DISPLACEMENT = 0.01, MINIMIZATION METHOD = POWELL, MIN_ENERGY_CHANGE = 0.05, NON_BONDED_RESET = 10, RESET_COUNT = 100, RMS_DISPLACEMENT = 0.001, RMS_GRADIENT = 0.05, SIMPLEX_ITERATIONS = 20, SIMPLEX_THRESHOLD = 1000, STATUS UPDATE = 1, TERMINATION· bdOPTION = ENERGY_CHANGE, THRESHOLD = –10.0. Atom types were assigned as follows: pyrrole nitrogens, Npl3; lactam nitrogens, N_{am}; carbonyl carbons, C.2; carbonyl oxygens, 0.2; carboxylic acid OH oxygens, 0.3; all other sp^2 carbons, C.2; and all sp^3 carbons, C.3. All bonds were assigned as formal double or single bonds.

The dipyrrinone units (Figure 3) of bilirubin-IXα and mesobilirubin-XIIIα were rotated independently about the central $-CH_2-$ at C_{10} (torsion angles ϕ_1 and ϕ_2, Figure 2) through 10° increments from 0° to 360°. (The $\phi_1 = 0°$, $\phi_2 = 0°$ conformer has a porphyrin-like shape, Figure 2.) In this procedure, the two torsion angles were held fixed at each increment, while the remainder of the molecular was relaxed to its minimum energy conformation using molecular mechanics. Our minimization routine starts by locking the two central torsion angles (ϕ_1 and ϕ_2) to the values we want to examine. This is followed by a molecular mechanics minimization to reduce any large steric interactions that may have developed from the angle rotations. The molecule then undergoes a molecular dynamics heating and cooling curve followed by a final molecular mechanics minimization to assure that the rotational conformer is in its lowest energy state. The molecular dynamics curve consists of heating the molecule to 20 K for 100 fs and then cooling to 10 K for 100 fs, 5 K for 100 fs, 2 K for 200 fs, 1 C for 200 fs, and 0.5 K for 300 fs. All values for atom types, bond angles, and cooling curve data were chosen by their ability to correctly reproduce bilirubin crystal structure data. The conformational energy maps were created using Wingz (Informix), and the ball and stick drawings were created from the atomic coordinates of the molecular dynamics structures using Müller and Falk's "Ball and Stick" program (Cherwell Scientific, Oxford, U.K.) for the Macintosh.

Acknowledgment. We thank the National Institutes of Health (HD-17779) for generous support of this work. R.V. Person is an R.C. Fuson Graduate Fellow and a Jerry and Betty Wilson Graduate Fellow. B.R. Peterson thanks the National Science Foundation for an REU undergraduate research fellowship.

(45) Shrout, D. P.; Puzicha, G.; Lightner, D. A. *Synthesis* **1992**, 328–332.

(46) Trull, F. R.; Lightner, D. A. *Arch. Biochem. Biophys.* **1992**, *298*, 710–714.